Modification Kit (Intergen, Purchase, NY, USA) (Saito *et al.*, 2001). This process converts unmethylated cytosine residues into uracil, whereas methylated cytosine residues remain unchanged (Frommer *et al.*, 1992). The treated DNA was resuspended in 50 μl of distilled water and amplified by PCR using primers specific for the DNA region, to analyse the status of methylation. After 45 cycles of the first PCR, nested PCR (45 cycles) was performed; the sequences of the primers for the seventh intron of the RFX1 gene were as follows: first sense, 5′-GGT TTT GGG TTA GTT TTA ATT TTT-3′; first antisense, 5′-TTC TCT AAA TCC TAA CCC TCT AA-3′; nested sense, 5′-GGT GGA GGT TTG GAG TTT-3′; nested antisense, 5′-ACA AAA ACA AAT ATA AAA ACA ACA-3′. The PCR products were subcloned into the pGEM-T Easy vector and sequenced.

Reporter gene assay

The seventh intron of the RFX1 gene containing a CpG island was subcloned into the pGL3-Promoter vector (Promega, Purchase, WI, USA), which contains an SV40 promoter upstream of the luciferase gene. The pGL3-Basic vector (Promega, Purchase, WI, USA), which lacks eucaryotic promoter and enhancer sequences, was used as a negative control vector, and the pGL3-Control vector (Promega, Purchase, WI, USA), which contains SV40 promoter and enhancer sequences, was used as a positive control vector. At 2 days after the gene transfection into U251 glioma cells using LipofectAMINE PLUS™ Reagent (Invitrogen, Carlsbad, CA, USA), the luciferase activity of 5×10^4 cells was measured with the Wallac ARVO™ SX 1420 multilabel counter (Perkin Elmer Life Sciences).

Treatment of cells with 5-aza-C and/or TSA

Human glioma U251 cells were plated at a low density, and 5-aza-C (500 nM; Sigma, St Louis, MO, USA) was added to the medium after 24 h. The drug-containing medium was replaced every 24 h for 3 days, with the addition of TSA (Maegawa *et al.*, 2001; Sekita *et al.*, 2001) (WAKO, Osaka, Japan) at 50 ng/ml for the last 24 h. After 4 days of culture, the total RNAs were isolated from the treated cells.

Thymidine uptake assay

Full-length human RFX1 cDNA digested from pHRFX1 (kindly provided by Dr W Reith) (Siegrist *et al.*, 1993) was subcloned into the mammalian expression vector pFLAG-CMV-2. The resultant plasmid, pFLAG-HRFX1, expressed the human RFX1 cDNA under the control of the CMV promoter and was tagged at its N-terminal with FLAG. At 1 day after the gene transfection into U251 glioma cells using LipofectAMINE PLUS™ Reagent, 5000 cells per well were replated on a 96-well plate, in quadruplicate. The cells were then cultured for 48 h and pulsed with [^{3}H]thymidine (1 μCi/well) for the last 24 h of incubation. [^{3}H]thymidine uptake was measured using a Top counter (Perkin Elmer Life Sciences).

Western blot analysis

Cell lysates were prepared using the RIPA buffer (1% NP-40, 0.1% sodium deoxycholate, 150 mM NaCl, 50 mM Tris-HCl (pH 7.5), 1 mM PMSF, and 0.2 U/ml aprotinin). Identical amounts of proteins (60 μg) were electrophoresed in 7% polyacrylamide gel under reducing conditions and transferred to a nitrocellulose membrane. The RFX1 protein was detected using an anti-RFX1 polyclonal antibody (Santa Cruz Biotechnology Inc.) diluted 1 : 250, followed by alkaline phosphatase-conjugated anti-goat IgG antibody diluted 1 : 500 (Sigma, St Louis, MO, USA).

Acknowledgements

We thank Mr Muramatsu and Mr Iizuka (Keio University School of Medicine) for their technical support. We are also grateful to Dr W Reith (University of Geneva Medical School) for providing us with the pHRFX1 plasmid. This work was supported by grants from grant-in-aid for Scientific Research from the Japanese Ministry of Education, Culture, Sports, Science and Technology (MT), the Keio University Medical Science Fund (MT), and grand-in-aid for Scientific Research on Priority Areas from the Japanese Ministry of Education, Culture, Sports, Science and Technology (MU).

References

Blin N and Stafford DW. (1976). *Nucleic Acids Res.*, **3**, 2303–2308.

Chen L, Smith L, Johnson MR, Wang K, Diasio RB and Smith JB. (2000). *J. Biol. Chem.*, **275**, 32227–32233.

Costello JF, Fruhwald MC, Smiraglia DJ, Rush LJ, Robertson GP, Gao X, Wright FA, Feramisco JD, Peltomaki P, Lang JC, Schuller DE, Yu L, Bloomfield CD, Caligiuri MA, Yates A, Nishikawa R, Su Huang H, Petrelli NJ, Zhang X, O'Dorisio MS, Held WA, Cavenee WK and Plass C. (2000). *Nat. Genet.*, **24**, 132–138.

Di Cristofano A, Pesce B, Cordon-Cardo C and Pandolfi PP. (1998). *Nat. Genet.*, **19**, 348–355.

Emery P, Durand B, Mach B and Reith W. (1996). *Nucleic Acids Res.*, **24**, 803–807.

Frommer M, McDonald LE, Millar DS, Collis CM, Watt F, Grigg GW, Molloy PL and Paul CL. (1992). *Proc. Natl. Acad. Sci. USA*, **89**, 1827–1831.

Fults D, Brockmeyer D, Tullous MW, Pedone CA and Cawthon RM. (1992). *Cancer Res.*, **52**, 674–679.

Gajiwala KS, Chen H, Cornille F, Roques BP, Reith W, Mach B and Burley SK. (2000). *Nature*, **403**, 916–921.

Gardiner-Garden M and Frommer M. (1987). *J. Mol. Biol.*, **196**, 261–282.

Hatada I, Hayashizaki Y, Hirotsune S, Komatsubara H and Mukai T. (1991). *Proc. Natl. Acad. Sci. USA*, **88**, 9523–9527.

Humphrey PA, Wong AJ, Vogelstein B, Friedman HS, Werner MH, Bigner DD and Bigner SH. (1988). *Cancer Res.*, **48**, 2231–2238.

Itano O, Ueda M, Kikuchi K, Shimazu M, Kitagawa Y, Aiura K and Kitajima M. (2000). *Oncogene*, **19**, 1676–1683.

Katan-Khaykovich Y and Shaul Y. (2001). *Eur. J. Biochem.*, **268**, 3108–3116.

Lindsay S and Bird AP. (1987). *Nature*, **327**, 336–338.

Maegawa S, Yoshioka H, Itaba N, Kubota N, Nishihara S, Shirayoshi Y, Nanba E and Oshimura M. (2001). *Mol. Carcinogen.*, **31**, 1–9.

Meehan RR, Lewis JD and Bird AP. (1992). *Nucleic Acids Res.*, **20**, 5085–5092.

Melki JR, Vincent PC and Clark SJ. (1999). *Cancer Res.*, **59**, 3730–3740.

Nakamura M, Yonekawa Y, Kleihues P and Ohgaki H. (2001). *Lab. Invest.*, **81**, 77–82.

Rasheed BK, Wiltshire RN, Bigner SH and Bigner DD. (1999). *Curr. Opin. Oncol.*, **11**, 162–167.

Saito Y, Kanai Y, Sakamoto M, Saito H, Ishii H and Hirohashi S. (2001). *Hepatology*, **33**, 561–568.

Sekita N, Suzuki H, Ichikawa T, Kito H, Akakura K, Igarashi T, Nakayama T, Watanabe M, Shiraishi T, Toyota M, Yoshie O and Ito H. (2001). *Jpn. J. Cancer Res.*, **92**, 947–951.

Sidransky D, Mikkelsen T, Schwechheimer K, Rosenblum ML, Cavanee W and Vogelstein B. (1992). *Nature*, **355**, 846–847.

Siegrist CA, Durand B, Emery P, David E, Hearing P, Mach B and Reith W. (1993). *Mol. Cell. Biol.*, **13**, 6375–6384.

Smiraglia DJ, Fruhwald MC, Costello JF, McCormick SP, Dai Z, Peltomaki P, O'Dorisio MS, Cavenee WK and Plass C. (1999). *Genomics*, **58**, 254–262.

Umezawa A, Yamamoto H, Rhodes K, Klemsz MJ, Maki RA and Oshima RG. (1997). *Mol. Cell. Biol.*, **17**, 4885–4894.

Whang YE, Wu X, Suzuki H, Reiter RE, Tran C, Vessella RL, Said JW, Isaacs WB and Sawyers CL. (1998). *Proc. Natl. Acad. Sci. USA*, **95**, 5246–5250.

Yamada KM and Araki M. (2001). *J. Cell Sci.*, **114**, 2375–2382.

Zardo G, Tiirikainen MI, Hong C, Misra A, Feuerstein BG, Volik S, Collins CC, Lamborn KR, Bollen A, Pinkel D, Albertson DG and Costello JF. (2002). *Nat. Genet.*, **32**, 453–458.

Squamous cell carcinoma of the liver originating from non-parasitic cysts after a 15 year follow-up

Hiroshi Yagi[a], Masakazu Ueda[a], Shigeyuki Kawachi[a], Minoru Tanabe[a], Kouichi Aiura[a], Go Wakabayashi[a], Motohide Shimazu[a], Mituie Sakamoto[b] and Masaki Kitajima[a]

Squamous cell carcinoma is an extremely rare primary liver tumour. A 42-year-old man presented at our hospital on 19 February 1986, with pain in the right upper quadrant of the abdomen and general fatigue, and reported an 8 year history of this complaint. Ultrasonography showed four cystic masses in the liver with a maximum diameter of 15 cm, one of which contained a solid component. A computed tomography (CT) scan confirmed a huge, predominantly cystic, mass in the liver with a small solid component and irregular wall. Calcifications were seen in the solid components. On 22 April 1986, a laparotomy was performed but the masses were too large to be removed. During 15 years of follow-up after the laparotomy, there had been no change seen in his abdominal CT scan. He subsequently arrived at our hospital again on 10 July 2001 with loss of appetite and of body weight. A CT scan showed a cyst in the liver of 25 cm in diameter with calcification that had a large solid part invading the liver. A post-mortem pathological dissection showed multiple cysts, the largest of which was 25 cm in diameter. They had large solid parts with calcification invading the liver. There were widespread metastatic lesions. Microscopic examination showed the tumour to be a well differentiated squamous cell carcinoma. To the best of our knowledge, this is the first report of a squamous cell carcinoma arising from 15 multiple non-parasitic hepatic cysts after a 15 year follow-up. Furthermore, 23 years had passed since the patient's symptoms appeared for the first time. *Eur J Gastroenterol Hepatol* **16:1051–1056 © 2004 Lippincott Williams & Wilkins**

European Journal of Gastroenterology & Hepatology 2004, 16:1051–1056

Keywords: squamous cell carcinoma, liver, non-parasitic cysts

[a]Department of Surgery and [b]Department of Pathology, Keio University School of Medicine, Tokyo, Japan.

Correspondence to Dr Masakazu Ueda, Department of Surgery, School of Medicine, Keio University, 35 Shinanomachi, Shinjuku-ku, Tokyo 160-8582, Japan.
Tel: +81 3 3353 1211 ext. 62334; fax: +81 3 3355 4707;
e-mail: m_ueda@sc.itc.keio.ac.jp

Received 18 June 2003
Accepted 12 January 2004

Introduction

Squamous cell carcinoma is an extremely rare primary liver tumour arising from chronic inflammatory conditions of non-parasitic hepatic cysts. We were able to find only 11 previously reported cases of squamous cell carcinoma arising from non-parasitic cysts. Our patient had had the symptoms from about 8 years before the first arrival and he died 15 years after a laparotomy. To the best of our knowledge, this is the first case report on primary squamous cell carcinoma, arising from multiple non-parasitic cysts of the liver, after a follow-up of 15 years.

Case report

A 42-year-old man presented with pain at our hospital on 19 February 1986, with pain in the right upper quadrant of the abdomen and general fatigue. The patient reported an 8 year history of this complaint. Physical examination revealed a right quadrant mass.

On admission, his temperature was 36.5°C and his liver was palpable four finger breadths below the costal margin. Laboratory studies showed the following values: haematocrit 42%; white cell count 6000; haemoglobin 13.7 mg/dl; direct bilirubin 0.5 mg/dl; total bilirubin 1.2 mg/dl; total cholesterol 185 mg/dl; serum aspartate transaminase 15 IU/l; alanine aminotransferase 28 IU/l; lactate dehydrogenase 320 IU/l; alkaline phosphatase 196 IU/l; total protein 7.7 g/dl; blood urea nitrogen 20.3 mg/dl; creatinine 1.2 mg/dl; uric acid 7.7 mg/dl; plasma retention rate of indocyanine green at 15 min 7.7%; carcinoembryonic antigen 1.4 ng/ml; alpha-fetoprotein 3 ng/ml; CA19-9 1380.0 U/ml.

Ultrasonography showed four cystic masses with a maximum diameter of 15 cm in segments 4, 5, 6, 7 and 8 of the liver. One of them contained a solid component (Fig. 1). A computed tomography (CT) scan confirmed a huge, predominantly cystic, mass in the liver with small solid components and an irregular wall, involving the porta hepatis causing intrahepatic biliary dilatation. Calcifications were seen in the solid components (Fig. 2). Angiography showed a hypovascular mass with scattered area of neovascularity in the right

0954-691X © 2004 Lippincott Williams & Wilkins

Fig. 1

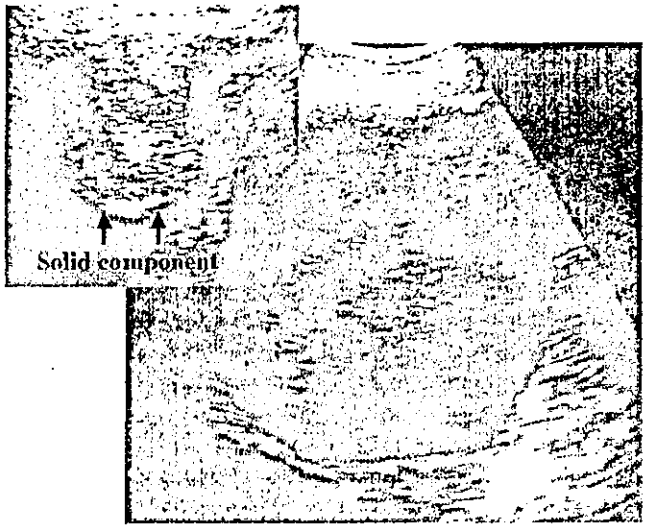

Abdominal ultrasonography shows four cystic masses in the liver with a maximum diameter of 15 cm in segments 4, 5, 6, 7 and 8. One of them contains a solid component. Dilatation of the intra-hepatic biliary duct can be seen.

Fig. 2

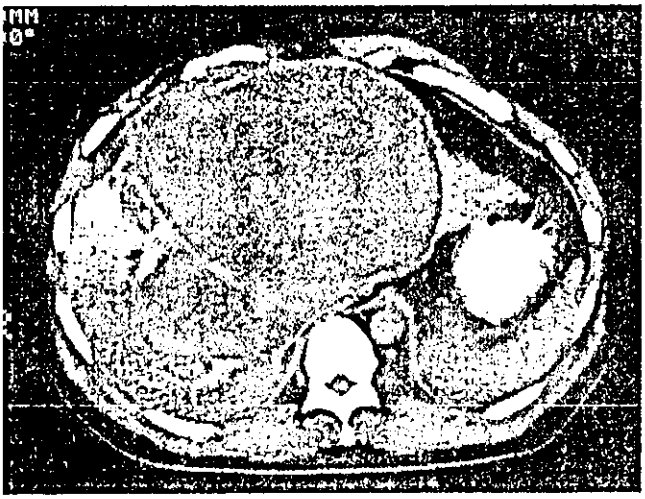

Abdominal computed tomography (CT) scan confirmed a huge, predominantly cystic mass in the liver with small solid components and irregular wall, involving the porta hepatis and causing intrahepatic biliary dilatation. Calcifications are seen in the solid components.

anterior hepatic artery (Fig. 3). A liver scintigram, using ^{99m}Tc-phytate, showed multiple defects. Fine-needle aspiration was performed under ultrasound guidance, which revealed no cancer cells.

The patient's clinical course is summarized in Table 1. On 22 April 1986, a laparotomy was performed. Intraoperatively, large cystic masses occupied the left medial segment, the right anterior segment and part of the

Fig. 3

Angiography shows a hypovascular mass with a scattered area of neovascularity in the right anterior hepatic artery.

right posterior segment of the liver with invasion into the right hepatic vein, and which contained a dark brown and non-serous fluid. We concluded that they were impossible to remove. In May 1986, during angiography, cisplatin (100 mg) was injected into the common hepatic artery. After that, cisplatin (100 mg) was injected three times (on 17 August 1986, 17 April 1987 and 24 August 1987). After the laparotomy, the patient had a CT scan every year which showed only a minor increase in the size of the tumour without any change in the solid component (Fig. 4). He lived a normal daily life for 15 years.

In December 2000 he developed a fever of 38°C and was treated with antibiotics at the ambulatory clinic. Because his fever failed to drop below 37°C and right upper abdominal pain appeared, he entered a regional hospital on 22 February 2001, but, on 24 March 2001, he discharged himself from the hospital because of his work. He entered the hospital again on 21 June 2001 with a loss of appetite and of body weight over the previous few weeks. On admission, his temperature was 38.5°C and the liver was palpable eight finger breadths below the costal margin. A CT scan showed the cyst with calcification in the liver of 25 cm in diameter, and the solid part was invading the liver (Fig. 5). In addition, there were multiple cysts contiguous to the biggest cyst, even ascites and bilateral pleural effusion. Laboratory studies showed the following values: white cell count 16 700; haemoglobin 5.9 mg/dl; total bilirubin 12.1 mg/dl; alkaline phosphatase 1217 IU/l; C-reactive protein 14.32 mg/dl; ammonia 102 μmol/l. These data suggested a radical redevelopment of the tumour, with hepatic failure and sepsis. He was moved to our hospital on 10 July 2001, following a strong request

Table 1 Clinical course from the first arrival

Situation	First Admission				During follow-up there was no particular change on CT			Ambulatory clinic	Entered a regional hospital	Discharged	Entered a regional hospital	Moved to our hospital	Died
	↓						↓	↓	↓	↓	↓	↓	↓
Therapy		Laparotomy	TAI	TAI	TAI	TAI			Antibiotics				
		↓	↓	↓	↓	↓			↓	↓			
Symptoms		Right upper quadrant pain						Fever up 38°C	37°C		Appetite loss		
	19 Feb 1986	22 Apr	16 May	17 Aug	17 Apr 1987	24 Aug	29 Feb 1996	18 Dec 2000	22 Feb 2001	24 Mar	21 June	10 July	14 July

CT, computed tomography; TAI, transcatheter arterial infusion.

Fig. 4

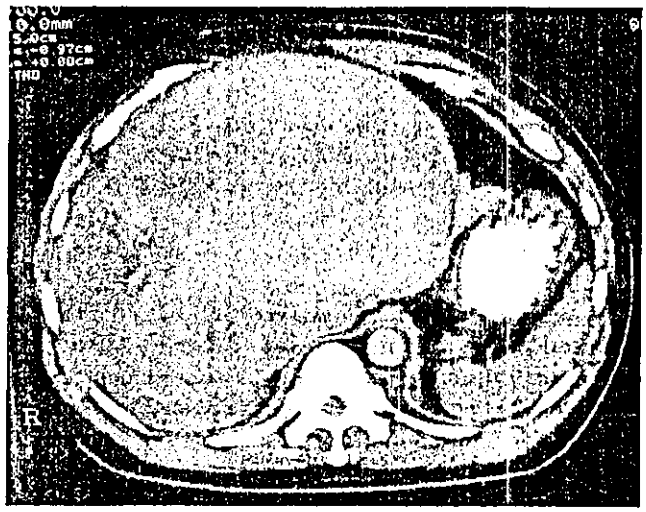

Abdominal CT scan in 1997 shows cystic masses with 16 cm maximum diameter. No change was seen in the solid component.

Fig. 5

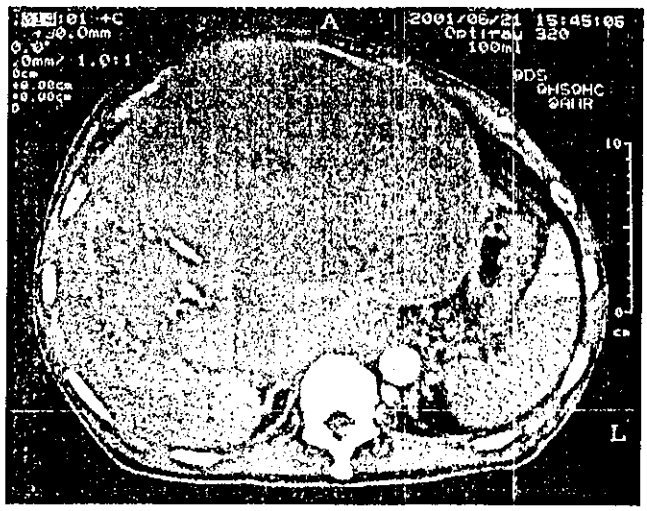

Abdominal CT scan in 2001 shows a cyst in the liver of about 25 cm in diameter and a large solid part invading the liver. There are also multiple cysts contiguous to that biggest cyst, even ascites and bilateral pleural effusion.

from his family. We treated him with antibiotics and cathecholamine but he died on 14 July.

A post-mortem pathological dissection showed multiple cysts ranging in size from 3 cm to 25 cm at the largest diameter. Each showed a granular brown surface with chronic inflammation and haemorrhagic foci, but only

focally lined by bile duct-type epithelium. The cyst had a large solid part with calcification, which had invaded the liver, the hepatic vein and the diaphragm. No replacing growth of carcinoma cells was encountered along the bile duct epithelium. The cysts contained a dark brown malodorous fluid. There was no evidence of cirrhosis in the remainder of the liver. There were widespread metastatic lesions from the tumour, including white metastatic nodules in the thoracic cavity, bilateral kidneys and adrenal glands.

Microscopic examination showed the tumour to be composed of infiltrating cords and sheets of mitotically active, well differentiated squamous cells characterized by large, hyperchromatic, pleomorphic nuclei and scant-to-moderate amounts of eosinophilic, occasionally vacuolated cytoplasm. Keratin pearls, individual cell keratinization, and intercellular bridges were prominent (Fig. 6). The tumour had penetrated multiple portal vein branches, and was contiguous with the cyst, but a transition from carcinoma *in situ* to invasive carcinoma was not identified.

Discussion

When we see multiple cysts in the liver which have an enhanced solid portion, it is usually diagnosed as cystadenoma or cystadenocarcinoma. According to Takayasu and colleagues [1], the incidence of biliary cystadenocarcinoma among hepatic malignant epithelial tumours is as low as 0.41% and more than 100 cases have been reported up to the present. Just as in our patient, the most common presenting symptoms are abdominal pain with a palpable mass. These lesions are believed to arise from benign cystadenomas, and show a multiseptal cystic mass that frequently has calcifications. Because of these characteristics, we first diagnosed our patient as having cystadenocarcinoma. We only knew our patient had a squamous cell carcinoma for the first time when we saw the pathology report.

Fig. 6

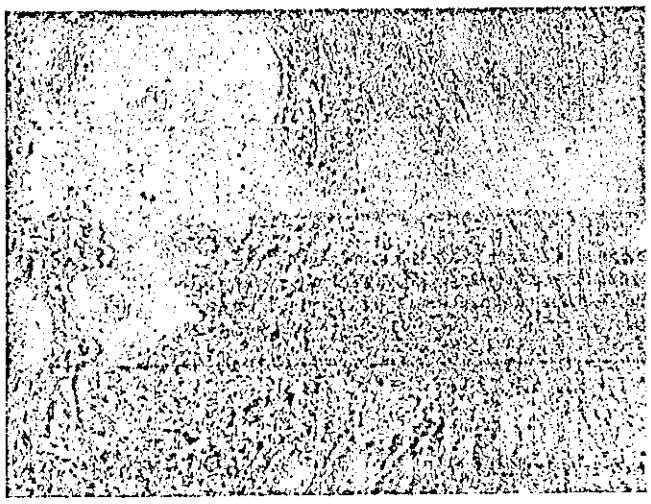

Microscopic examination shows the tumour is composed of well differentiated squamous cells characterized by large, hyperchromatic, pleomorphic nuclei and scant-to-moderate amounts of eosinophilic, occasionally vacuolated cytoplasm. Keratin pearls, individual cell keratinization, and intercellular bridges are prominent.

This is the first report of a squamous cell carcinoma arising from multiple non-parasitic hepatic cysts after a 15 year follow-up. Furthermore, 23 years had passed since the symptoms had appeared for the first time. It is very interesting that our patient had a small solid component from his first arrival, and though it showed no change during 15 years, it suddenly progressed dramatically. Though it was not clear whether it was the effect of the chemotherapy, the sudden malignant change appeared in the solid component that had no malignancy at first. We were unable to find a documented case showing widespread metastatic dissemination of the tumour like this case.

Squamous cell carcinoma deriving from benign non-parasitic hepatic cyst is extremely rare. In our review of the literature, there are only 11 cases of squamous cell carcinoma (Table 2). Although congenital hepatic cysts are three to five times more common in women than in men [2], there were six men in these cases including ours. Their median age was 63 years. While the cyst was solitary in 10 other cases, Pliskin *et al.* found advanced carcinoma in two of three different cysts in the same patient [3]. Ours is the second case arising from multiple cysts. Tumour sizes ranged from 2.5 cm to 25 cm in diameter and our patient had the biggest tumour amongst the other cases. Though we could not resect the tumours because of their size and location, six patients (50%) were treated operatively. The median survival time was 5 months in these cases. In five of these instances, there had been invasion of the surrounding liver and only one had metastasis to another organ (lymph nodes) [4]. Our patient is the first to have metastasis to multiple organs including the heart and lung. We could not detect any signs of metastasis to the heart and lungs before he died because the CT scan showed no thoracic metastasis in 1999. Then, he suddenly developed high fever and soon after coming to our hospital he died.

Various types of epithelial lining can be found in these cases. There was benign squamous epithelium in eight cases, and bile duct type epithelium in the remaining three cases [3–5]. Metaplastic epithelium was additionally reported in three of these 11 cases [3,6,7].

The aetiology was most probably secondary squamous metaplasia due to chronic inflammation of the biliary

Table 2 **Reported cases of primary squamous cell carcinoma originating from liver cysts**

Case no.	First author and year	Age/gender	Therapy	Cysts	Tumour size (cm)	Survival	Histology
1	Edmondson, 1958 [14]	56/M	Unknown	Solitary	Unknown	Unknown	Unkown
2	Greenwood, 1972 [4]	37/M	Laparotomy	Solitary	Unknown	2 months	Lymph node metastasis Invading the liver Benign squamous epithelium Bile duct-type epithelium
3	Bloustein, 1976 [13]	30/M	1. Laparotomy with drainage 2. R-Y drainage of cyst 3. Right hepatectomy	Solitary	7.2 × 5.4 × 5.4	6 months	Invading the liver Benign squamous epithelium
4	Gresham, 1985 [6]	78/M	Drainage of ascites	Solitary	20 × 10	2 months	No invasion Squamous epithelium dysplastic in many areas
5	Lynch, 1988 [11]	63/M	1. Unroofing of cyst and drainage 2. Subtotal cystectomy	Solitary	8	6 months	Invading the liver Benign squamous epithelium
6	Nieweg, 1992 [9]	62/F	Laparotomy	Solitary	11 × 12 × 1 5	5 months	Fibrous tissue with focal squamous differentiation
7	Pliskin, 1992 [3]	82/F	?	Multiple	4, 4, 2.5	13 days	Invading the liver Bile duct-type epithelium Benign high grade dysplasia, *in situ*, well keratinizing
8	Banbury, 1994 [5]	59/F	Right hepatectomy	Solitary	14 × 11 × 10	16 months alive	No invasion Squamous epithelium Bile duct-type epithelium
9	Weimann, 1996 [7]	74/F	Right hemihepatectomy including partial resection of the right diaphragm	Solitary	12 × 10	4.5 years alive	No invasion Carcinomatous epithelium next to inflammatory changes
10	Doctor, 1998 [12]	68/F	1. S4, 5 segmentectomy 2. Chemotherapy	Solitary	7	Unknown	Unknown
11	Monteagudo, 1998 [10]	71/F	Cystostomy	Solitary	9 × 16	1 month	Invading the liver Squamous epithelium
12	Present case	58/M	1. Laparotomy 2. Transarterial chemotherapy	Multiple	3–25	15 years	Invading the liver Metastasis to heart, lung, kidneys, adrenal Carcinomatous epithelium next to inflammatory changes

lined cysts or ducts and subsequent neoplastic transformation [4]. This is consistent with the histology in our case, with carcinomatous epithelium next to subsequent chronic inflammation of the biliary lined cysts. Because pathological findings showed that the tumour was completely composed of well differentiated squamous cell carcinoma with no metaplastic lesions, and probably under the influence of the chemotherapy, the greater part of the cyst wall had an inflammatory epithelium with wide calcification, and we could not find the origin of the tumour, pathologically. Abdominal CT showed that the tumour appeared to be secondary, arising from the area where the first solid component had existed.

The surgical management of solitary non-parasitic cysts of the liver has not been rigidly defined. Hepatic anatomical and local resections, drainage, marsupialization, and aspiration have all been described as giving satisfactory results [8]. Furthermore, the incidence of malignancy in solitary non-parasitic hepatic cysts is exceedingly low. Therefore, major hepatic resections are not believed to be warranted when simple removal is precluded by the attachment of the hepatic cyst to vital structures, or when there is extensive multilobular involvement. However, it is possible that, as additional reports of malignancy arising in such cysts are accumulated, these recommendations may be revised.

Once squamous cell carcinoma arises from the lining of the hepatic cysts, the prognosis is extremely grave, and thus complete surgical excision should be performed rather than simple drainage, marsupialization, or partial excision. But it often progresses despite all forms of surgical and medical management.

Conclusion

Our case and the previously cited cases illustrate the difficulty in making a correct preoperative diagnosis. CT seems to be one of the most valuable pre-operative investigations.

Survival from the time of diagnosis has not exceeded 1 year, regardless of the form of treatment utilized. Our case is thought to be valuable because the longest recorded survival was 16 months after laparotomy. It is also interesting that, finally, the tumour suddenly progressed and showed widespread metastasis to heart, lung, kidneys and adrenals.

References

1 Takayasu K, Muramatsu Y, Moriyama N, Yamada T, Hasegawa H, Hirohashi S, Ichikawa T, *et al.* Imaging diagnosis of bile duct cystadenocarcinoma. *Cancer* 1988; 61:941–946.

2 Lauffer JM, Baer CA, Maurer CA, Stoupis CH, Zimmerman A, Buchler MW. Biliary cystadenocarcinoma of the liver: the need for complete resection. *Eur J Cancer* 1998; 34:1845–1851.

3 Pliskin A, Cualing H, Stenger RI. Primary squamous cell carcinoma originating in congenital cysts of the liver – report of a case and review of the literature. *Arch Lab Med* 1992; 116:105–107.

4 Greenwood N, On WM. Primary squamous-cell carcinoma arising in a solitary non-parasitic cyst of the liver. *J Pathol* 1972; 107:145–148.

5 Banbury J, Condon KC. Primary squamous cell carcinoma within a solitary nonparasitic hepatic cyst. *J Surg Oncol* 1994; 57:210–212.

6 Gresham GA, Rue LW. Squamous cell carcinoma of the liver. *Hum Pathol* 1985; 16:413–416.

7 Weimann A, Klempnauer J. Squamous cell carcinoma of the liver originating from a solitary non-parasitic cyst: case report and review of the literature. *Hepato-biliary Surgery* 1996; 10:45–49.

8 Ameriks J, Appleman H, Frey C. Malignant nonparasitic cyst of the liver. *Ann Surg* 1972; 176:713–717.

9 Nieweg O, Sloof MJ, Grond J. A case of primary squamous cell carcinoma of the liver arising in a solitary cyst. *Hepato-biliary Surgery* 1992; 5:203–208.

10 Monteagudo M, Vidal G. Squamous cell carcinoma and infection in a solitary hepatic cyst. *Eur J Gastroenterol Hepatol* 1998; 10:1051–1053.

11 Lynch MJ, McLeod MK, Weatherbee L, Gilsdorf JR, Giuce KS, Eckhauser FE. Squamous cell cancer of the liver arising from a solitary benign nonparasitic cyst. *Am J Gastroenterol* 1988; 83:426–431.

12 Doctor N, Dafnios N, Jones A, Davidson BR. Primary squamous carcinoma of liver: presentation as liver abscess. *Ind J Gastroenterol* 1998; 17:28–29.

13 Bloustein PA, Silverberg SG. Squamous cell carcinoma originating in an hepatic cyst – case report and review of the hepatic cyst–carcinoma association. *Cancer* 1976; 38:2002–2005.

14 Edmondson HA. *Tumors of the Liver and Intrahepatic Bile Ducts. Atlas of Tumor Pathology.* Washington, DC: Armed Forces Institute of Pathology; 1958, pp. 109–110.

THE JOURNAL OF BIOLOGICAL CHEMISTRY
© 2004 by The American Society for Biochemistry and Molecular Biology, Inc.

Vol. 279, No. 40, Issue of October 1, pp. 41521–41528, 2004
Printed in U.S.A.

Induction of Hypoxia-inducible Factor 1 Activity by Muscarinic Acetylcholine Receptor Signaling*

Received for publication, May 10, 2004, and in revised form, July 26, 2004
Published, JBC Papers in Press, July 26, 2004, DOI 10.1074/jbc.M405164200

Kiichi Hirota‡§¶, Ryo Fukuda§, Satoshi Takabuchi‡‖, Shinae Kizaka-Kondoh, Takehiko Adachi‡, Kazuhiko Fukuda‖, and Gregg L. Semenza§**

*From the ‡Department of Anesthesia, The Tazuke Kofukai Medical Research Institute Kitano Hospital, 2-4-20, Ohgimachi, Kita-ku, Osaka 530-8480, Japan, §Program in Vascular Cell Engineering, The Johns Hopkins University School of Medicine, Baltimore, MD 21205, the ‖Department of Anesthesia, Kyoto University Hospital, Kyoto University, Sakyo-ku, Kyoto 606-8507, Japan, and the **COE Formation for Genomic Analysis of Disease Model Animals with Multiple Genetic Alterations, Kyoto University Graduate School of Medicine, Yoshida-Konoe-cho, Sakyo-ku, Kyoto 606-8507, Japan*

Hypoxia-inducible factor-1 (HIF-1) is a master regulator of cellular adaptive responses to hypoxia. Levels of the HIF-1α subunit increase under hypoxic conditions. Exposure of cells to growth factors, prostaglandin, and certain nitric oxide donors also induces HIF-1α expression under non-hypoxic conditions. We demonstrate that muscarinic acetylcholine signals induce HIF-1α expression and transcriptional activity in a receptor subtype-specific manner using HEK293 cells transiently overexpressing each of M1-M4 muscarinic acetylcholine receptors. The muscarinic signaling pathways inhibited HIF-1α hydroxylation and degradation and induced HIF-1α protein synthesis that was confirmed by pulse labeling studies. Muscarinic signal-induced HIF-1α protein and HIF-1-dependent gene expression were blocked by treating cells with inhibitors of phosphatidylinositol 3-kinase, MAP kinase kinase, or tyrosine kinase signaling pathways. Dominant-negative forms of Ras and/or Rac-1 significantly suppressed HIF-1 activation by muscarinic signaling. Signaling via M1- and M3- but not M2- or M4-AchRs promote accumulation and transcriptional activation of HIF-1α. We conclude that muscarinic acetylcholine signals activate HIF-1 by both stabilization and synthesis of HIF-1α and by inducing the transcriptional activity of HIF-1α.

Hypoxia activates a number of genes that are important in cellular and tissue adaptation to low oxygen conditions (1). These genes include erythropoietin, glucose transporters, glycolytic enzymes, and vascular endothelial growth factor (VEGF).[1] The hypoxic expression of these different genes is controlled at the transcriptional level by the ubiquitously expressed transcription factor hypoxia-inducible factor 1 (HIF-1) (2). HIF-1 is a heterodimer composed of a constitutively expressed HIF-1β subunit and an inducibly expressed HIF-1α subunit (3). The regulation of HIF-1 activity occurs at multiple levels *in vivo*. Among these, the mechanisms regulating HIF-1α protein expression and transcriptional activity have been most extensively analyzed (4). The von Hippel-Lindau tumor-suppressor protein (VHL) has been identified as the HIF-1α-binding component of a ubiquitin-protein ligase that targets HIF-1α for proteasomal degradation in non-hypoxic cells (5). Under hypoxic conditions, the hydroxylation of specific proline and asparagine residues in HIF-1α is inhibited due to substrate (O_2) limitation, resulting in HIF-1α protein stabilization and transcriptional activation (6, 7). The iron chelator deferrioxamine (DFX) inhibits the prolyl and asparaginyl hydroxylases, which contain Fe^{2+} at their catalytic sites, causing HIF-1α stabilization and transactivation under normoxic conditions (6, 8).

Physiological stimuli other than hypoxia can also induce HIF-1 activation and the transcription of hypoxia-inducible genes (9–14). Signaling via the HER2/neu or IGF-1 receptor-tyrosine kinase induces HIF-1 expression by an oxygen-independent mechanism. HER2/neu activation increases the rate of HIF-1α protein synthesis via phosphatidylinositol 3-kinase (PI3K) and the downstream serine-threonine kinases AKT (protein kinase B) and FRAP (FKBP/rapamycin-associated protein; also known as mTOR (mammalian target of rapamycin)) (12). IGF-1-induced HIF-1α synthesis is dependent upon both the PI3K and MAP kinase (MAPK) pathways (13). The effect of HER2/neu signaling on HIF-1α protein translation is dependent upon the presence of the 5′-untranslated region of HIF-1α mRNA. In addition to growth factors, prostaglandin E_2, thrombin, angiotensin II, and 5-hydroxytryptamine induce HIF-1 activation (11, 14). Notably, cellular receptors for these agents are heterotrimeric guanine nucleotide binding (G) protein-coupled receptors (GPCR). Moreover, a constitutively active GPCR encoded by the Kaposi's sarcoma-associated herpes virus/human herpes virus 8 is reported to induce HIF-1 activation in a MAPK-dependent manner (15).

In this study, we demonstrate that muscarinic acetylcholine receptor (mAchR)-mediated signals induce HIF-1 activation in a receptor-subtype specific manner using HEK293 cells transfected with various types of mAchR. Signaling via M1- and M3- but not M2- or M4-AchRs promote accumulation and transcriptional activation of HIF-1α. We also provide evidence that the activation is dependent on Gα- or Gβγ-dependent and tyrosine kinase, MAPK, and PI3K activity.

* This work was supported in part by a grant-in-aid for scientific research from the Ministry of Education, Culture, Sports, Science and Technology (to K. H. and T. A.). The costs of publication of this article were defrayed in part by the payment of page charges. This article must therefore be hereby marked "*advertisement*" in accordance with 18 U.S.C. Section 1734 solely to indicate this fact.

¶ To whom correspondence should be addressed: Dept. of Anesthesia, The Tazuke Kofukai Medical Research Institute Kitano Hospital, 2-4-20, Ohgimachi, Kita-ku, Osaka 530-8480. Tel.: 81-6-6312-8831; Fax: 81-6-6312-8867; E-mail: hif1@mac.com.

[1] The abbreviations used are: VEGF, vascular endothelial growth factor; HIF-1, hypoxia-inducible factor 1; GPCR, G protein-coupled receptor; mAchR, muscarinic acetylcholine receptor; CCH, carbachol; MAP, mitogen-activated protein; MAPK, MAP kinase; DFX, desferrioxamine; PI3K, phosphatidylinositol 3-kinase; VHL, von Hippel-Lindau; HRE, hypoxia responsive element; TAD, transactivation domain; HA, hemagglutinin; GST, glutathione *S*-transferase; Ab, antibody; CHX, cycloheximide; IGF, insulin-like growth factor; β-gal, β-galactosidase; HEK, human embryonic kidney cells; MEK, MAPK kinase.

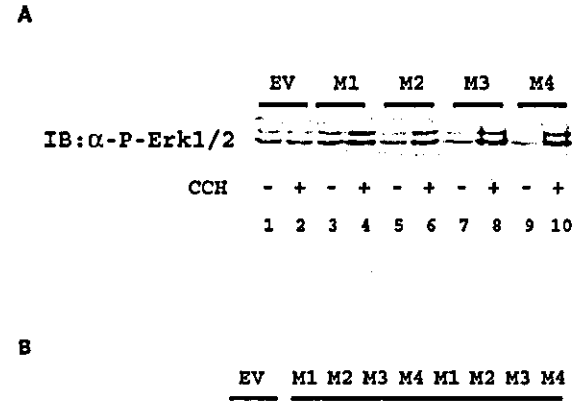

FIG. 1. **Effect of carbachol on HIF-1α levels in muscarinic acetylcholine receptor-expressing HEK293 cells.** *A*, HEK293 cells were transiently transfected with an empty vector (*EV*) or expression plasmids encoding M1-M4-muscarinic acetylcholine receptors (500 ng) and treated with 100 μM carbachol (CCH) for 20 min. Cells were harvested, and lysates were subjected to immunoblot assay (*IB*) using an Ab that recognize the phosphorylated forms of p42/p44 MAPK. *B*, transfected cells expressing mAchR were treated with CCH or DFX (*lane 2*) for 4 h. Cell lysates were subjected to immunoblot assay using anti-HIF-1α or anti-HIF-1β Abs. *C–F*, M1-expressing cells were treated with CCH (100 μM) in the presence or absence of atropine (atr) (5 μm) (*C*), with 100 nM to 100 μM CCH (*D*), with CCH for 1–8 h (*E*) or with CCH, DFX, or CCH and atr (*F*), and analyzed for HIF-1α expression by immunoblot assay using anti-HIF-1α Ab.

FIG. 2. **Effect of CCH on gene expression.** HEK293 cells transfected with EV or an expression vector encoding M1-AchR were treated with 0, 10, or 100 μM CCH, or DFX for 24 h and then total RNA was isolated from them. Expression of VEGF and HIF-1α mRNA was analyzed by blot hybridization using VEGF (*top panel*) or HIF-1α (*middle panel*) cDNA probe following RNA transfer from an ethidium bromide-stained gel (*bottom panel*; 28 S and 18 S rRNA indicated).

EXPERIMENTAL PROCEDURES

Cell Culture and Reagents—HEK293 cells and human dopaminergic neuroblastoma SK-N-SH cells were maintained in Dulbecco's modified Eagle's medium supplemented with 10% fetal bovine serum, 100 units/ml penicillin, and 100 μg/ml streptomycin. DFX was obtained from Sigma. Carbachol (CCH), cycloheximide (CHX), genistein, LY294002, PD98059, SB203580 and GF109203X were obtained from Calbiochem (San Diego, CA).

Plasmid Constructs—Expression vectors for porcine M1-M4 AChRs were described previously (16, 17). Expression vectors pGAL4/HIF-1α-(531–826), pGAL4/HIF-1α-(531–575), pGAL4/HIF-1α-(726–826) and pGAL4/HIF-1α-(786–826) were described previously (8). Plasmid p2.1 contains a 68-bp hypoxia response element (HRE) from the *ENO1* gene inserted upstream of an SV40 promoter in the luciferase reporter plasmid pGL2-Promoter (Promega) and p2.4 contains a 3-bp mutation in the HRE (18). Plasmid pVEGF-KpnI contains nucleotides −2274 to +379 of the *VEGF* gene inserted into luciferase reporter pGL2-Basic (Promega) (19). The reporter pG5E1bLuc contains five copies of a GAL4 binding site upstream of a TATA sequence and firefly luciferase coding sequences. The expression plasmid pCR3.1-HA-FIH-1 and a plasmid encoding a dominant negative form of HIF-1α (pCEP4-HIF-1αΔNBΔAB) were described previously (20, 21). The expression plasmid pCH-NLS-HIF1α-(548–603)-LacZ was described elsewhere (22). Plasmids encoding constitutively activated from of heterotrimeric G protein α-subunits pcDNA3-Gαq Q209L, pcDNA3-Gα12 Q229L, and pcDNA3-Gα13 Q226L were kindly provided by Dr. Manabu Negishi (Kyoto University, Kyoto, Japan) (23). Plasmids encoding bovine $G\beta_1$ and $G\gamma_2$ are made from $G\beta_1$ and pcDNA3.1 (−) and $G\gamma_2$ and pcDNA3.1(+), respectively (24). Plasmids encoding a dominant negative form of Ras (Ras^{N17}) or Rac1 ($Rac1^{N17}$) were generous gifts from Dr. Kaikobad Irani (Johns Hopkins University, Baltimore, MD) (25) and Dr. Kozo Kaibuchi (Nagoya University, Nagoya, Japan) (26), respectively. A dominant negative form of MEK1, MEK1(A) and a dominant negative form of MEK5, MEK5(A) were from Dr. Eisuke Nishida (Kyoto University) (27, 28).

Hypoxic Treatment—Tissue culture dishes were transferred to a modular incubator chamber (Billups-Rothenberg, Del Mar, CA) which was flushed with 1% O_2, 5% CO_2, 94% N_2, sealed, and placed at 37 °C (29).

Immunoblot Assays—Whole cell lysates were prepared by incubating cells for 30 min in cold radioimmune precipitation assay (RIPA) buffer containing 2 mM dithiothreitol, 1 mM $NaVO_3$, and Complete protease inhibitor™ (Roche Applied Science) (29). Samples were centrifuged at 10,000 × *g* to pellet cell debris. For HIF-1α and HIF-1β, 100-μg aliquots were fractionated by 7.5% SDS-polyacrylamide gel electrophoresis and subjected to immunoblot assay using mouse monoclonal antibodies against HIF-1α or HIF-1β (H1α67 and H1β234; Novus Biologicals, Littleton, CO) at 1:1000 dilution. Signal was developed using the ECL reagent (Amersham Biosciences). For analysis of phosphorylated proteins, HEK293 cells were treated with CCH and 50-μg aliquots were analyzed using specific antibodies (1:1000 dilution) (Cell Signaling

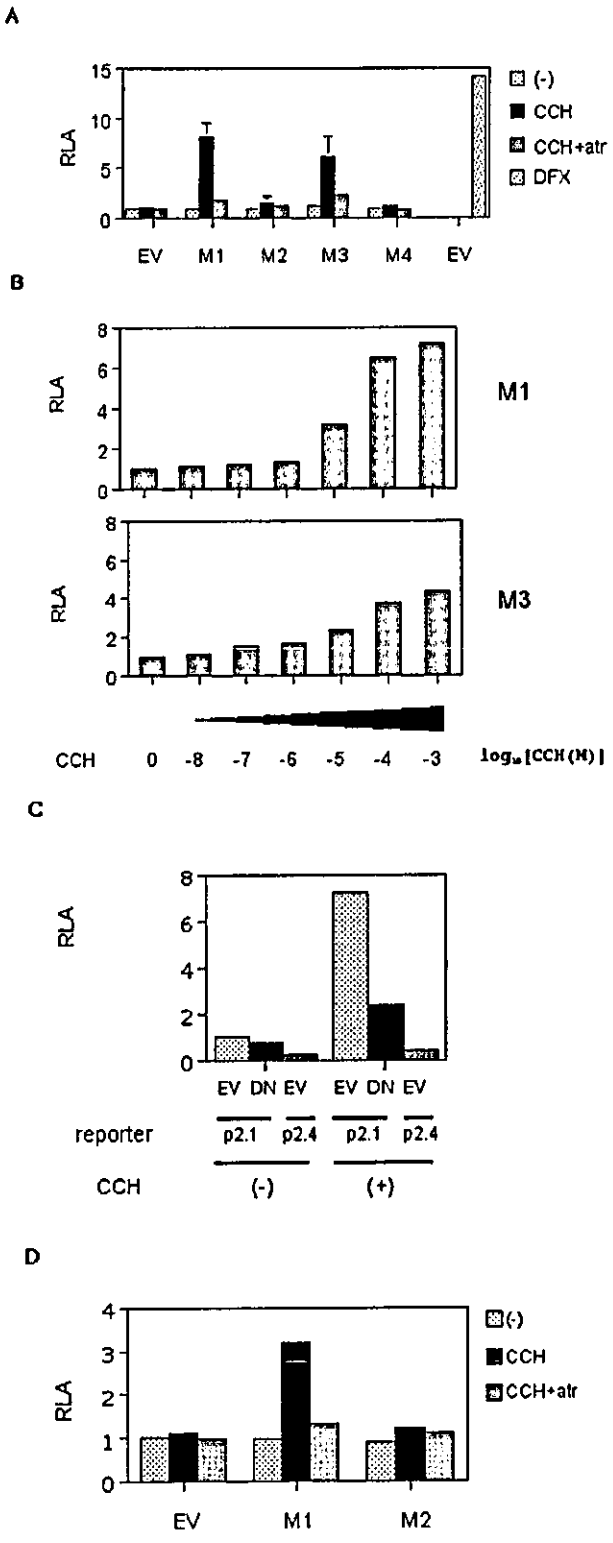

FIG. 3. **Effect of muscarinic signaling on HRE-dependent gene expression.** *A*, HEK293 cells were transfected with pTK-RL (10 ng), encoding *Renilla* luciferase, and HRE reporter p2.1 (150 ng), encoding firefly luciferase, with expression vector (300 ng) encoding a muscarinic AchR or EV. After 6 h, cells were treated or not treated with CCH (100 μM) or DFX (100 μM) for 16 h and then harvested for luciferase assays. The ratio of firefly:*Renilla* luciferase activity was determined and normalized to the value obtained from untreated cells transfected with empty vector to obtain the relative luciferase activity (*RLA*). *B*, HEK293 cells were transfected with pTK-RL, p2.1, and either M1-AchR (*upper*) or M3-AchR expression vector. After 6 h, cells were treated with the indicated doses of CCH for 16 h and then harvested for luciferase assays. *C*, HEK293 ells were co-transfected with M1-AchR, p2.1 or mutant HRE reporter p2.4, pTK-RL, and expression vector encoding either no protein (*EV*) or a dominant negative form of HIF-1α (*DN*). After 6 h, cells were treated with 100 μM CCH for 16 h and then harvested for luciferase assays. *D*, HEK293 cells were transfected with pTK-RL, *VEGF* promoter reporter pVEGF-KpnI, and either M1- or M2-AchR plasmid. After 6 h, cells were treated with 100 μM CCH alone or plus 5 μM atropine for 16 h and then harvested for luciferase assays.

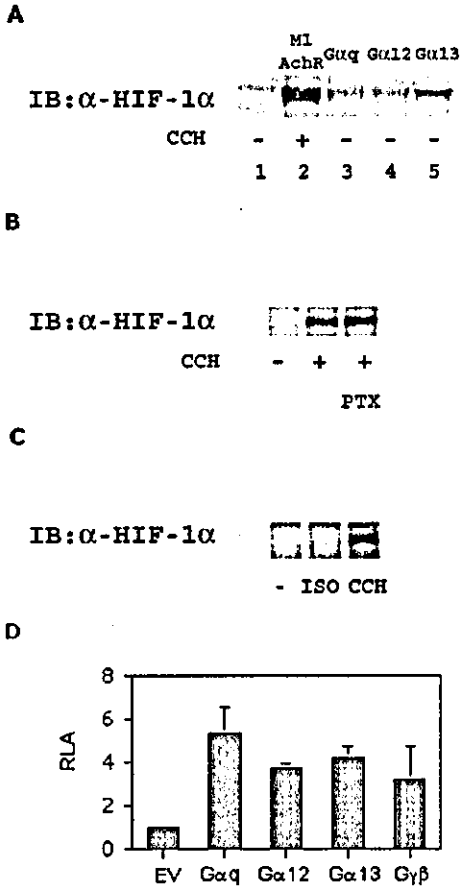

FIG. 4. **Involvement of G proteins in HIF-1α accumulation.** *A*, HEK293 cells were transfected with plasmid encoding a constitutively activated form of $G\alpha_q$, $G\alpha_{12}$, or $G\alpha_{13}$. After 24 h, cells were harvested, and lysates were subjected to immunoblot assay using anti-HIF-1α Ab. *B* and *C*, HEK293 cells expressing M1-AchR were treated with CCH alone or plus pertussis toxin (PTX) (*B*), or treated with isoproterenol (ISO; *lane 2*) or CCH (*lane 3*) (*C*) and analyzed for HIF-1α protein expression. *D*, HEK293 cells expressing M1-AchR were transfected with pTK-RL, HRE reporter p2.1, and expression vector encoding a constitutively activated form of $G\alpha_q$, $G\alpha_{12}$, $G\alpha_{13}$, or $G\gamma\beta$. Transfected cells were incubated for 24 h, harvested, and lysates were subjected to luciferase assays.

Technology, Beverly, MA). Signal was developed using the ECL reagent (Amersham Biosciences).

Inhibitor Treatments—PD98059, SB203580, LY294002, GF109203X, or genistein was added 1 h before exposure to CCH or 1% O_2. CHX was added to the medium of HEK293 cells that were treated with CCH, or DFX for 4 h, and whole cell extracts were prepared at 15, 30, and 60 min (12, 13).

RNA Blot Hybridization—Total RNA was extracted from HEK293 cells using TRIzol reagent (Invitrogen) 24 h after CCH stimulation and 48 h after transfection of expression plasmid encoding AchR. 10-μg aliquots of RNA were fractionated by electrophoresis in 1.5% agarose, 2.2 M formaldehyde gels, transferred to Hybond N +membranes (Amersham Biosciences), and hybridized with a ^{32}P-labeled human HIF-1α or VEGF cDNA probe as described previously (13).

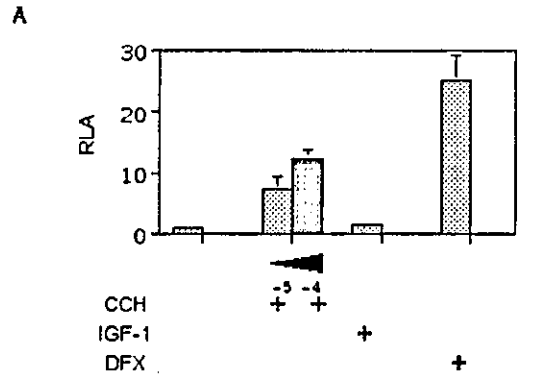

FIG. 5. **Effect of CCH, DFX, and IGF-1 on HIF-1α protein stability and synthesis.** *A*, HEK293 cells were transfected with M1-AchR, plasmid pCH-NLS-HIF-1α-(574–603)-LacZ and pGL-Control vector, which is a SV40 promoter- and enhancer-driven luciferase expression plasmid. Cells were treated with 100 μM (−4), 10 μM (−5) CCH, 100 ng/ml IGF-1, or 100 μM DFX for 12 h and subjected to β-gal assay. Normalized β-galactosidase activity is indicated in the figure. *B*, analysis of HIF-1α stability. HEK293 cells transfected with EV or M1-AchR plasmid were exposed to 100 μM CCH (*top*), 100 μM DFX (*middle*), or 100 ng/ml IGF-1 (*bottom*) for 4 h and then CHX was added to a final concentration of 100 μM. The cells were incubated for 0–60 min, and whole cell lysates were subject to immunoblot assay using anti-HIF-1α Ab. *C*, pulse labeling of HEK293 cells. Serum-starved cells expressing M1-AchR were pretreated with no drug, 100 μM CCH, or 100 ng/ml IGF-1 for 30 min in Met-free medium. [^{35}S]Met-Cys was added, and the cells were incubated for 40 min prior to preparation of cell lysates and immunoprecipitation of HIF-1α (*upper*). Parallel to the pulse label experiment, expression of HIF-1α mRNA was examined by RT-PCR (*lower*).

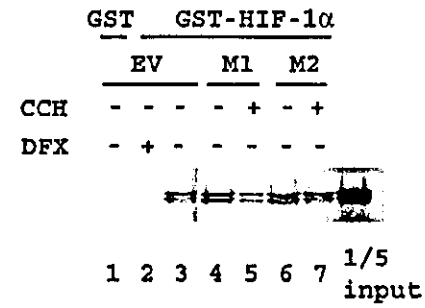

FIG. 6. **Analysis of interaction of HIF-1α and VHL.** GST or GST-HIF-1α-(429–608) fusion protein was incubated with *in vitro*-translated and ^{35}S-labeled VHL in the presence of phosphate-buffered saline (*lanes 1* and *2*) or lysates prepared from M1-expressing HEK293 cells that were untreated (*lane 3*) or exposed to 100 μM CCH (*lane 4*) or from M2-expressing HEK293 cells that were untreated (*lane 5*) or exposed to 100 μM CCH (*lane 6*). Glutathione-Sepharose beads were used to capture GST or GST-HIF-1α and the presence of bound VHL in the samples was determined by PAGE and autoradiography. One-fifth of the input VHL protein was also analyzed.

Reporter Gene Assays—Reporter assays were performed in HEK293 cells as described previously (29–31). Cells were transferred to 24-well plates at a density of 5×10^4 cells per well on the day before transfection. FuGENE 6 reagent (Roche Applied Science) was used for transfection. For luciferase assay, each mAchR, the reporter gene plasmid, and the control plasmid pTK-RL (Promega), containing a thymidine kinase promoter upstream of *Renilla reniformis* luciferase coding sequences, were pre-mixed with the transfection reagent. In each assay the total amount of DNA was held constant by addition of empty vector. After treatment, the cells were harvested and the luciferase activity was determined using the Dual-Luciferase Reporter Assay System (Promega). The ratio of firefly to *Renilla* luciferase activity was determined. For each experiment, at least two independent transfections were performed in triplicate. β-galactosidase (β-gal) activity was determined using a commercial assay system (Roche Applied Science) (32). To normalize β-gal activity of each sample, pGL-Control plasmid was co-transfected with a β-gal-coding plasmid. Net β-gal count of each sample was divided by its luciferase count and normalized mean count ± S.D. of three independent transfections is shown as relative activity.

Metabolic Labeling Assay—The protocol is described elsewhere (12). Briefly, HEK293 cells were plated in a 10-cm dish, and transfected with M1-AchR plasmid, and 18 h later the cells were serum-starved for 20 h. The cells were pretreated with 100 μM CCH or IGF-1 for 30 min in methionine-free Dulbecco's modified Eagle's medium. [^{35}S]Met-Cys was added to a final concentration of 0.3 mCi/ml, and the cells were pulse-labeled for 20–40 min and then harvested. Whole cell extracts were prepared, and 1 mg of extract was precleared with 60 μl of protein A-Sepharose for 1 h. Twenty microliters of anti-HIF-1α antibody H1α67 was added to the supernatant and rotated overnight at 4 °C. Forty microliters of protein A-Sepharose was added, rotated for 2 h at 4 °C, pelleted, and washed five times with 1 ml of radioimmune precipitation assay buffer. The samples were analyzed by SDS-polyacrylamide gel electrophoresis. The gel was dried and exposed to x-ray film.

In Vitro HIF-1α-VHL Interaction Assay—[^{35}S]Methionine-labeled VHL protein was synthesized *in vitro* and glutathione *S*-transferase (GST)-HIF-1α-(429–608) fusion protein was expressed in *E. coli* as described previously (20). HEK293 cells expressing M1- or M2-AchR were treated with CCH or DFX for 4 h prior to lysate preparation. GST-HIF-1α-(429–608) was preincubated with 10 μl of the HEK293 cell lysate for 30 min at 30 °C. 5-μl aliquots of the GST-HIF-1α-(429–608) preincubation and VHL *in vitro* translation reactions were mixed in 150 μl of NETN buffer (150 mM NaCl, 0.5 mM EDTA, 20 mM Tris-HCl (pH 8.0), 0.5% (v/v) Nonidet P-40). After 90 min at 4 °C, 20 μl of glutathione-Sepharose-4B (Amersham Biosciences) was added. After 30 min of mixing on a rotator, beads were washed three times with NETN buffer. Proteins were eluted in 2× SDS sample buffer, fractionated by SDS-PAGE, and detected by autoradiography.

RESULTS

Muscarinic Acetylcholine Receptors Induce HIF-1 Activity in a Receptor Subtype-specific Manner under Non-hypoxic Conditions—Because HEK293 cells express only low levels of mAchRs (33), it is possible to examine the effect of individual mAchR signaling on HIF-1 activation by overexpression of each mAchR. HEK293 cells were transfected with expression plasmid encoding the M1-, M2-, M3-, or M4-AchR and stimulated by the addition of the cholinergic agonist CCH. As shown in Fig. 1*A*, $p42^{ERK2}$/$p44^{ERK1}$ MAPKs were activated in response to treatment with CCH (100 μM) (*lanes 4*, *6*, *8*, and *10*). CCH simulation also induced transcriptional activation of Elk-1 in mAchR-expressing HEK293 cells (data not shown). Together, these data demonstrate that each mAchR subtype was functionally expressed in HEK293 cells. Furthermore, the levels of

ERK1/2 phosphorylation in response to CCH stimulation were similar, suggesting that the different mAchRs were expressed at comparable levels.

Using this system we investigated impact of mAchR stimulation on activation of HIF-1. 100 μM CCH increased HIF-1α protein levels in M1- or M3-AchR- but not in M2- or M4-AchR-expressing HEK293 cells (Fig. 1*B*). In contrast, HIF-1β protein levels were not affected by the binding of CCH to mAchR in HEK293 cells. The induction of HIF-1α expression was inhibited by atropine, demonstrating that the effect is receptor agonist-specific (Fig. 1*C*). The M1- or M3-AchR signal induced the accumulation of HIF-1α in a CCH dose-dependent manner to 100 nM (Fig. 1*D*). In M1-transfected HEK293 cells exposed to CCH (100 μM), HIF-1α protein levels peaked at 4 h (Fig. 1*E*). We next investigated involvement of mAchR in HIF-1α protein accumulation in SK-N-SH human neuroblastoma cells, which endogenously express M3-AchR. Treatment with CCH (100 μM) induced accumulation HIF-1α protein in 4 h and this accumulation was inhibited by treatment with atropine (Fig. 1*F*). Thus mAchR-mediated signals induced HIF-1α protein accumulation under non-hypoxic conditions.

M1- or M3-AchR Stimulation Activates HIF-1-dependent Gene Expression—We examined the impact of mAchR system on HIF-1-dependent gene expression. As shown in Fig. 2, *VEGF* gene expression was induced in M1-AchR-expressing HEK293 cells exposed to CCH (100 μM) or to the iron chelator DFX. The expression of HIF-1α mRNA was not affected by any treatment.

Next, HEK293 cells were transfected with reporter plasmid p2.1, which contains a HIF-1-dependent HRE, or p2.4, which contains a mutated, non-functional HRE. Stimulation of M1- or M3-AchR with CCH induced HRE-dependent expression comparably to 100 μM DFX treatment (Fig. 3*A*). The activation was CCH dose-dependent (Fig. 3*B*). In contrast, the reporter p2.4 was not activated by the treatment. Expression of a dominant negative form of HIF-1α markedly reduced p2.1 reporter gene expression, demonstrating that gene activation was both HRE- and HIF-1-specific (Fig. 3*C*). CCH treatment of cells expressing M1-AchR also induced expression of the pVEGF-KpnI reporter, which contains promoter sequences encompassing nucleotides −2274 to +379 relative to the transcription start site of the *VEGF* gene. In contrast, CCH had no effect on *VEGF* promoter activity in cells transfected with expression vector M2-AchR or empty vector (Fig. 3*D*).

Involvement of G Proteins in M1- or M3-AchR Stimulation—Because mAchRs are G protein-coupled receptors, we examined involvement of G proteins in the activation of HIF-1. Because M1- or M3-AchR mainly couples with $G\alpha_q$ protein in HEK293 cells (33, 34), we first examined involvement of $G\alpha_q$ in the process. Expression of a constitutively activated form of $G\alpha_q$ ($G\alpha_q$-Q209L) induced the accumulation of HIF-1α protein (Fig. 4*A*, *lane 3*) in HEK293 cells. Expression of $G\alpha_{12}$-Q229L or $G\alpha_{13}$-Q226L also induced the accumulation of HIF-1α (*lanes 4* and *5*). M1-AchR-mediated HIF-1α accumulation was not affected by treatment with pertussis toxin, which blocks interaction of $G\alpha_i$ GTPase with receptors (Fig. 4*B*). Stimulation of the endogenous β-adrenergic receptor with the β-adrenergic agonist isoproterenol did not induce HIF-1α protein accumulation, suggesting that $G\alpha_s$-mediated signaling did not contribute to HIF-1α accumulation (Fig. 4*C*) (35). Expression of a constitutively activated form of $G\alpha_q$-, $G\alpha_{12}$-, $G\alpha_{13}$-, or Gβγ-induced HRE-dependent reporter gene expression in HEK293 cells (Fig. 4*D*).

M1-AchR Stimulation Stabilizes β-Galactosidase Fused to the O_2-dependent Degradation Domain of HIF-1α—We examined the impact of M1-AchR-mediated signaling on the stability

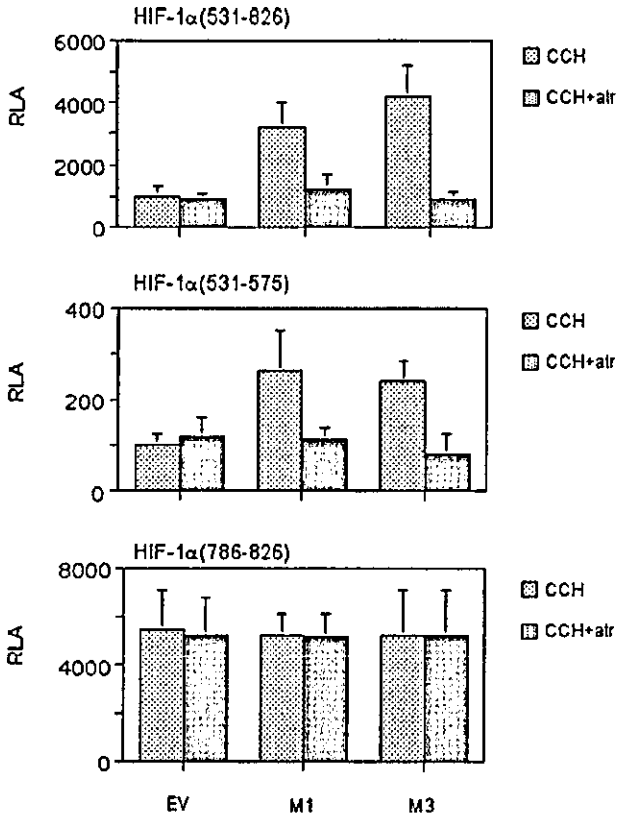

FIG. 7. **Effects of muscarinic signaling on HIF-1α transactivation domain function.** Constructs encoding the DNA-binding domain (amino acids 1–147) of the yeast transcription factor GAL4 fused to the indicated amino acids of HIF-1α were analyzed for their ability to transactivate reporter gene pG5E1bLuc, which contains five GAL4-binding sites. HEK293 cells were co-transfected with muscarinic receptors (200 ng), pTK-RL (10 ng), GAL4E1bLuc (150 ng), and GAL4-HIF-1α fusion protein expression plasmids (200 ng). Cells were exposed to CCH (100 μM) for 16 h and harvested. The ratio of firefly:*Renilla* luciferase activity was determined and normalized to the value obtained from untreated cells transfected with plasmid encoding GAL4-(1–147) to obtain the relative luciferase activity (RLA).

of HIF-1α protein by transfecting cells with expression vector pCH-NLS-HIF1α-(548–603)-LacZ, which encodes a fusion protein consisting of β-gal and the HIF-1α sequences encompassing the hydroxylation site at Pro-564. The levels of this protein, which can be monitored by measuring β-gal activity, are negatively regulated by O_2-dependent hydroxylation, ubiquitination, and proteasomal degradation (22). HEK293 cells transfected with M1-AchR and pCH-NLS-HIF1α-(548–603)-LacZ were treated with CCH, DFX, or IGF-1 and lysates were analyzed for β-gal activity. As shown in Fig. 5*A*, CCH (100 μM) stimulation induced β-gal activity although to a lesser extent than DFX. In contrast, IGF-1 stimulation did not significantly induce β-gal activity. These data suggest that M1-AchR signaling results in stabilization of HIF-1α protein.

To further investigate whether mAchR signaling affected HIF-1α protein half-life, mAchR-expressing HEK293 cells were treated with CCH, IGF-1, or DFX for 4 h to induce HIF-1α expression, CHX was added to block ongoing protein synthesis, and cell lysates were prepared for immunoblot assay (Fig. 5*B*). In the presence of CHX, the half-life of HIF-1α was more than 60 min in DFX-treated cells, ~30 min in CCH-treated cells, and less than 15 min in IGF-1-treated cells. These results indicate that M1-AchR stimulation induced accumulation of HIF-1α by increasing protein half-life.

To analyze the rate of HIF-1α synthesis, serum-starved

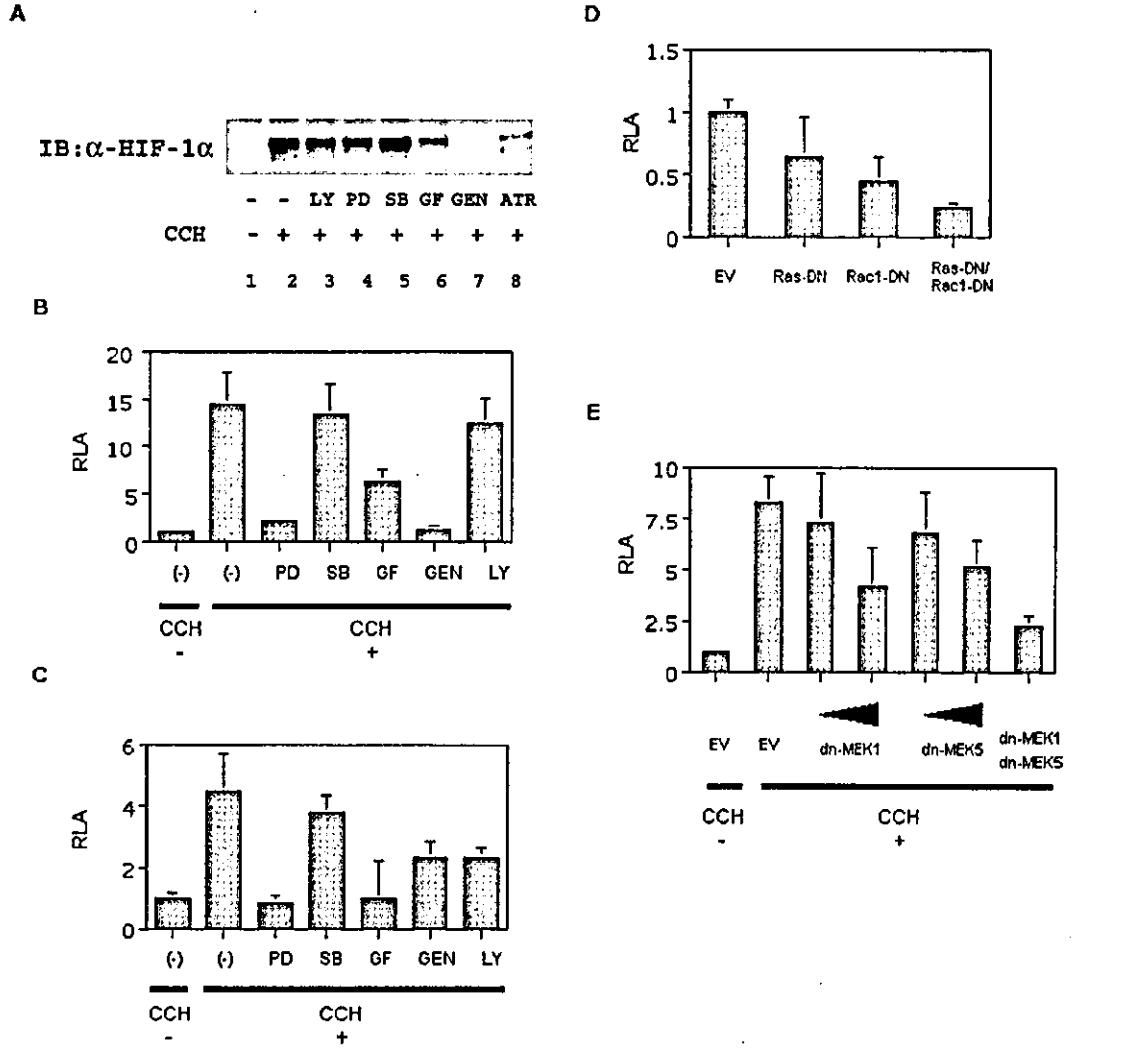

FIG. 8. **Analysis of signal transduction pathways involved in the induction of HIF-1 by muscarinic receptors.** *A*, M1-expressing HEK293 cells were exposed to vehicle (*lane 1*) or 100 μM CCH in the presence of no kinase inhibitor (*lane 2*) or a 1-h pretreatment with 50 μM LY294002 (*LY*), 50 μM PD98059 (*PD*) (*lane 4*), 25 μM SB203580 (*SB*) (*lane 5*), 50 μM GF109203X (*GF*) (*lane 6*), 100 μM genistein (*GEN*) (*lane 7*), or 5 μM atropine (*ATR*) (*lane 8*). Cells were harvested after 4 h for analysis of HIF-1α protein. *B* and *C*, M1-expressing HEK293 cells were subjected to reporter gene assay using p2.1 (*B*) or pGAL4/HIF-1α-(531–826) and pG5E1bLuc (*C*). Cells were exposed to vehicle or 100 μM CCH in the presence of no kinase inhibitor or co-treatment with 50 μM PD, 25 μM SB, 50 μM GF, 100 μM GEN, or 50 μM LY. Cells were harvested after 16 h for analysis. *D* and *E*, M1-expressing HEK293 cells were subjected to reporter gene assay using p2.1 with dominant negative (*DN*) forms of the G proteins Ras and/or Rac1 (*D*) or a dominant negative form of MEK1 or MEK5 (*E*). After 6 h, cells were treated with 100 μM CCH for 16 h and then harvested for luciferase assays.

HEK293 cells were pretreated with CCH or IGF-1 for 30 min and then pulse-labeled with [^{35}S]Met-Cys for 40 min, followed by immunoprecipitation of HIF-1α (Fig. 5*C*). In contrast to control serum-starved cells, ^{35}S-labeled HIF-1α was clearly increased in CCH-treated cells as well as IGF-1-treated cells (Fig. 5*C*, *upper*). Expression of HIF-1α mRNA was not affected during treatment (*lower*). Thus, both the cycloheximide and metabolic labeling experiments provide evidence for increased synthesis of HIF-1α in response to M1-mediated signal.

AchR Signaling Inhibits the Interaction of HIF-1α and VHL—Incubation of a GST-HIF-1α-(429–608) fusion protein with control lysate from untreated cells resulted in prolyl hydroxylation of HIF-1α and interaction with VHL (Fig. 6, *lane 1*). Lysate from DFX-treated 293 cells did not promote the interaction of GST-HIF-1α with VHL (*lane 2*). Lysate from CCH-treated M1-AchR-expressing cells was less effective in promoting the interaction (*lane 5*) than lysate from M1-AchR expressing cells without CCH treatment (*lane 4*). In contrast, lysates from M2-AchR-expressing cells promoted the interaction of GST-HIF-1α with VHL regardless of whether they were exposed to CCH or not (*lanes 6* and *7*).

mAchR Signaling Stimulates the Transcriptional Activity of HIF-1α—Two independent transactivation domains have been localized to amino acid residues 531–575 (TAD-N) and 786–826 (TAD-C) of HIF-1α (8, 20). Because it has been shown that steady-state levels of the fusion proteins containing GAL4 DNA-binding domain and HIF-1α TAD are similar under hypoxic and non-hypoxic condition, these GAL4-HIF-1α fusion proteins can be utilized to analyze HIF-1α TAD activity independent of any effects on protein expression. Activity of TAD-N is hypoxia-induced whereas TAD-C is constitutively active. M1- or M3-AchR stimulation enhanced gene expression mediated by GAL4-HIF-1α-(531–826), which contains both TAD-N and TAD-C (Fig. 7). GAL4-HIF-1α-(531–575)-mediated gene expression is also stimulated by M1- or M3-AchR, indicating that TAD-N function is regulated by mAchR signaling. The activity of GAL4-HIF-1α-

(786–826) was not affected by mAchR stimulation.

Effect of Kinase Inhibitors on AchR-mediated HIF-1 Activation—To investigate further the molecular mechanisms whereby muscarinic receptors activate HIF-1, M1-AchR-expressing HEK293 cells were stimulated by CCH under treatment with LY294002, PD98059, SB203580, GF109203X, or genistein which are selective pharmacologic inhibitors of PI3K, MEK, p38 MAPK, PKC, and tyrosine kinase activity, respectively. As shown in Fig. 8*A*, genistein almost completely inhibited HIF-1α accumulation induced by CCH (*lane 7*) similar to the effect of atropine (*lane 8*). GF109203X (*lane 6*) partially inhibited HIF-1α accumulation (lane 6), whereas treatment with LY294002 (*lane 3*), PD98059 (*lane 4*), or SB203580 (*lane 5*) had little or no effect.

Next, we investigated the effect of the inhibitors on HRE-dependent gene expression using the HRE-dependent p2.1 reporter (Fig. 8*B*). Genistein or PD98059 almost completely suppressed the gene expression by CCH. GF109203X had a partial inhibitory effect. In contrast, treatment with LY294002 or SB203580 did not have any inhibitory effect. The transcriptional activity of HIF-1α was examined using pGAL4/HIF-1α-(531–826) and pG5E1bLuc (Fig. 8*C*). PD98059 or GF109203X almost completely suppressed HIF-1α TAD activation induced by CCH. In contrast, treatment with genistein, LY294002, or SB203580 did not block TAD function induced by CCH.

Previously, we demonstrated that small G protein Ras and Rac1 are involved in hypoxia-induced HIF-1 activation process (29). We next examined involvement of Ras and Rac1 in the CCH-induced HIF-1 activation (Fig. 8*D*). Expression of dominant negative forms of Ras (Ras^{N17}) or Rac1 ($Rac1^{N17}$) inhibited CCH-induced HRE-dependent gene expression in M1-AchR-expressing HEK293 cells. Expression of a dominant negative form of MEK1 or MEK5 also inhibited CCH-induced gene expression (Fig. 8*E*), which is consistent with the observed effects of PD98059 in Fig. 8*B*.

DISCUSSION

Molecular cloning studies have revealed the existence of five distinct muscarinic receptor subtypes referred to as M1-M5 (33). The M1-M5 receptors are members of the GPCR superfamily. Although even numbered receptors (M2 and M4) are selectively coupled to G proteins of the $G\alpha_i/G\alpha_o$ family, the odd-numbered receptors (M1, M3, and M5) are preferentially linked to $G\alpha_q/G\alpha_{11}$ proteins (16, 17). Our results demonstrate that muscarinic acetylcholine receptor-mediated signals induce HIF-1 activation under non-hypoxic conditions in a receptor subtype-specific manner. Only odd numbered receptors induced HIF-1α protein expression and transcriptional activity in a receptor-ligand-dependent manner in HEK293 cells. Expression of a constitutively activated form of $G\alpha_q$, $G\alpha_{12}$, $G\alpha_{13}$, or $G\beta\gamma$ is sufficient to induce accumulation of HIF-1α and HIF-1-mediated transcription (Fig. 4*D*). The selective effect of M1- or M3- *versus* M2- or M4-AchR signaling does not appear to be related to the level of receptor expression based on the ERK activation (Fig. 1*A*).

HIF-1α protein expression level is determined by the balance between protein synthesis and degradation (12, 13). CCH stimulation of M1-expressing HEK293 cells increased the half-life of HIF-1α protein compared with that in IGF-1-treated cells although the effect was less than that induced by DFX, which inhibits HIF-1α prolyl hydroxylases (Fig. 5*B*). CCH also induced stabilization of HIF-1α-(548–603)-β-gal fusion protein in HEK293 cells expressing M1-AchR (Fig. 5*A*). Moreover, lysate of M1-expressing HEK293 cells stimulated by CCH was less effective than lysate from unstimulated cells in promoting the interaction between HIF-1α and VHL. Together, these results

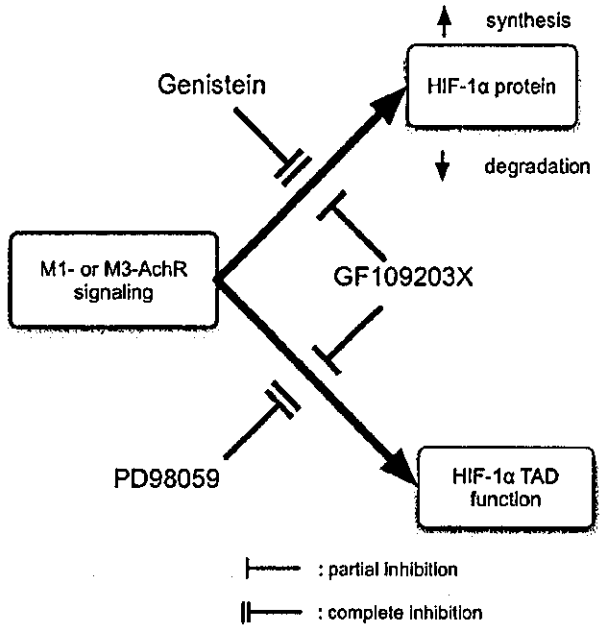

FIG. 9. **Schematic representation of mAchR signaling to HIF-1.** The effects of pharmacologic inhibitors suggest that multiple signaling pathways downstream of muscarinic receptors stimulate HIF-1α protein expression and HIF-1α transactivation domain (*TAD*) function.

suggest that M1-AchR signaling regulates HIF-1α hydroxylation, ubiquitination, and/or proteasomal degradation. However, the effect of mAchR signaling on HIF-1α accumulation is not explained fully by the stabilization mechanism, because the effect on the half-life of HIF-1α is much less that that induced by DFX (Fig. 5*B*). We have reported that certain growth factors such as IGF-1 (12, 13), prostaglandin E_2 (14), and the nitric oxide donor NOC18 increase the rate of HIF-1α protein synthesis rather than increasing the stability of HIF-1α. The pulse-labeling data (Fig. 5*C*) indicate that mAchR stimulation also increases the rate of HIF-1α synthesis. The dual effects on both synthesis and stability account for the high levels of HIF-1α induced by mAchR signaling.

Src family kinases are also activated by $G\alpha_q/G\alpha_{11}$-coupled receptors via the proline-rich tyrosine kinase 2 (PKY2) (36). v-Src and Ras^{V12} signaling in RCC4 and 786–0 cells has been shown to stabilize HIF-1α by inhibiting hydroxylation of Pro-564 (37). The effects of dominant negative forms of Ras and Rac1 (Fig. 8*D*) suggest that similar mechanisms may be involved in AchR-mediated HIF-1 activation. We demonstrate that the activation of HIF-1 in response to muscarinic signaling is suppressed by the PKC inhibitor GF109203X or the tyrosine kinase inhibitor genistein. (Fig. 8). M1 and M3 muscarinic receptors stimulate phospholipase C_β, which hydrolyzes phosphatidylinositol 4,5-bisphosphate to generate the second messengers diacylglycerol and inositol 1,4,5-triphosphate (34) causing PKC activation. In fact, genistein or GF109203X inhibits M1-AchR-mediated HIF-1α accumulation. Taken together, the pathway may lead to HIF-1α accumulation (Fig. 9). Regulation of HIF-1 activity involves changes in both the protein expression and transcriptional activity of HIF-1α (8, 20, 29). Our data analyzing transactivation mediated by Gal4-HIF-1α-TAD fusion proteins demonstrate that muscarinic receptor signaling also induces HIF-1α TAD activity under non-hypoxic conditions. A major determinant of TAD function is the interaction between HIF-1α and the coactivators p300/CBP, which regulated by O_2-dependent hydroxylation of Asn-803 by FIH-1 (7, 20). TAD activity is also regulated by a

MAPK-dependent mechanism (29, 38) that enhances recruitment of p300/CBP (39). The MEK inhibitor PD98059, which is a selective pharmacologic inhibitor of MEK1 and MEK5, blocked muscarinic signal-induced HIF-1, suggesting a link between muscarinic signaling, MEK/ERK, and HIF-1α. The data presented in Fig. 8*E* suggest that MEK1 and MEK5 cooperatively play a critical role in this process. The signal transduction pathway leading from muscarinic receptor activation to HIF-1α TAD activation is also sensitive to the PKC inhibitor GF109203X.

The M1-M4 receptors are widely expressed throughout the central and peripheral nervous systems (34). The M1 receptor is found in greatest abundance in the cortex and hippocampus where it constitutes 40–50% of the total mAchR. Activation of HIF-1 may provide a mechanism to increase glucose uptake and/or perfusion in response to increased neuronal activity via increased transcription of genes encoding glucose transporters and angiogenic factors such as VEGF. In PC12 pheochromocytoma cells, HIF-1 serves as a neuroprotective factor against amyloid β peptide, which is involved in the pathogenesis of Alzheimer's disease (40). Notably, the M1 receptor is coupled with processing the amyloid precursor protein (41). Finally, mice with a deletion of the HIF-1 binding site within the HRE of the *Vegf* gene develop motor neuron degeneration similar to amyotrophic lateral sclerosis (42), indicating an important role for HIF-1 in VEGF-mediated motor neuron survival. Further studies are required to determine whether HIF-1 activation by muscarinic receptor signaling may play an important role in regulating cell survival in neurodegenerative disorders.

Acknowledgments—We thank Drs. Toshihide Nukada, Kozo Kaibuchi, Eisuke Nishida, and Manabu Negishi for providing plasmid vectors.

REFERENCES

1. Hochachka, P. W., Buck, L. T., Doll, C. J., and Land, S. C. (1996) *Proc. Natl. Acad. Sci. U. S. A.* **93**, 9493–9498
2. Iyer, N. V., Kotch, L. E., Agani, F., Leung, S. W., Laughner, E., Wenger, R. H., Gassmann, M., Gearhart, J. D., Lawler, A. M., Yu, A. Y., and Semenza, G. L. (1998) *Genes Dev.* **12**, 149–162
3. Wang, G. L., Jiang, B. H., Rue, E. A., and Semenza, G. L. (1995) *Proc. Natl. Acad. Sci. U. S. A.* **92**, 5510–5514
4. Semenza, G. L. (2000) *J. Appl. Physiol.* **88**, 1474–1480
5. Semenza, G. L. (2001) *Cell* **107**, 1–3
6. Epstein, A. C., Gleadle, J. M., McNeill, L. A., Hewitson, K. S., O'Rourke, J., Mole, D. R., Mukherji, M., Metzen, E., Wilson, M. I., Dhanda, A., Tian, Y. M., Masson, N., Hamilton, D. L., Jaakkola, P., Barstead, R., Hodgkin, J., Maxwell, P. H., Pugh, C. W., Schofield, C. J., and Ratcliffe, P. J. (2001) *Cell* **107**, 43–54
7. Lando, D., Peet, D. J., Gorman, J. J., Whelan, D. A., Whitelaw, M. L., and Bruick, R. K. (2002) *Genes Dev.* **16**, 1466–1471
8. Jiang, B. H., Zheng, J. Z., Leung, S. W., Roe, R., and Semenza, G. L. (1997) *J. Biol. Chem.* **272**, 19253–19260
9. Jiang, B. H., Agani, F., Passaniti, A., and Semenza, G. L. (1997) *Cancer Res.* **57**, 5328–5835
10. Zhong, H., Chiles, K., Feldser, D., Laughner, E., Hanrahan, C., Georgescu, M. M., Simons, J. W., and Semenza, G. L. (2000) *Cancer Res.* **60**, 1541–1545
11. Richard, D. E., Berra, E., and Pouysségur, J. (2000) *J. Biol. Chem.* **275**, 26765–26771
12. Laughner, E., Taghavi, P., Chiles, K., Mahon, P. C., and Semenza, G. L. (2001) *Mol. Cell. Biol.* **21**, 3995–4004
13. Fukuda, R., Hirota, K., Fan, F., Jung, Y. D., Ellis, L. M., and Semenza, G. L. (2002) *J. Biol. Chem.* **277**, 38205–38211
14. Fukuda, R., Kelly, B., and Semenza, G. L. (2003) *Cancer Res.* **63**, 2330–2334
15. Sodhi, A., Montaner, S., Patel, V., Zohar, M., Bais, C., Mesri, E. A., and Gutkind, J. S. (2000) *Cancer Res.* **60**, 4873–4880
16. Fukuda, K., Kubo, T., Akiba, I., Maeda, A., Mishina, M., and Numa, S. (1987) *Nature* **327**, 623–625
17. Fukuda, K., Higashida, H., Kubo, T., Maeda, A., Akiba, I., Bujo, H., Mishina, M., and Numa, S. (1988) *Nature* **335**, 355–358
18. Semenza, G. L., Jiang, B. H., Leung, S. W., Passantino, R., Concordet, J. P., Maire, P., and Giallongo, A. (1996) *J. Biol. Chem.* **271**, 32529–32537
19. Forsythe, J. A., Jiang, B. H., Iyer, N. V., Agani, F., Leung, S. W., Koos, R. D., and Semenza, G. L. (1996) *Mol. Cell. Biol.* **16**, 4604–4613
20. Mahon, P. C., Hirota, K., and Semenza, G. L. (2001) *Genes Dev.* **15**, 2675–2685
21. Jiang, B. H., Rue, E., Wang, G. L., Roe, R., and Semenza, G. L. (1996) *J. Biol. Chem.* **271**, 17771–17778
22. Harada, H., Hiraoka, M., and Kizaka-Kondoh, S. (2002) *Cancer Res.* **62**, 2013–2018
23. Katoh, H., Aoki, J., Yamaguchi, Y., Kitano, Y., Ichikawa, A., and Negishi, M. (1998) *J. Biol. Chem.* **273**, 28700–28707
24. Nakamura, K., Nukada, T., Haga, T., and Sugiyama, H. (1994) *J. Physiol.* **474**, 35–41
25. Irani, K., Xia, Y., Zweier, J. L., Sollott, S. J., Der, C. J., Fearon, E. R., Sundaresan, M., Finkel, T., and Goldschmidt-Clermont, P. J. (1997) *Science* **275**, 1649–1652
26. Kuroda, S., Fukata, M., Kobayashi, K., Nakafuku, K., Nomura, N., Iwamatsu, A., and Kaibuchi, K. (1996) *J. Biol. Chem.* **271**, 23363–23367
27. Gotoh, I., Fukuda, M., Adachi, M., and Nishida, E. (1999) *J. Biol. Chem.* **274**, 11874–11880
28. Kamakura, S., Moriguchi, T., and Nishida, E. (1999) *J. Biol. Chem.* **274**, 26563–26571
29. Hirota, K., and Semenza, G. L. (2001) *J. Biol. Chem.* **276**, 21166–21172
30. Itoh, T., Namba, T., Kazuhiko, F., Semenza, L. G., and Hirota, K. (2001) *FEBS Lett.* **509**, 225–229
31. Ang, S. O., Chen, H., Hirota, K., Gordeuk, V. R., Jelinek, J., Guan, Y., Liu, E., Sergueeva, A. I., Miasnikova, G. Y., Mole, D., Maxwell, P., Stockton, D. W., Semenza, G. L., and Prchal, J. T. (2002) *Nat. Genetics* **32**, 614–621
32. Hirota, K., Murata, M., Itoh, T., Yodoi, J., and Fukuda, K. (2001) *J. Biol. Chem.* **276**, 25963–25968
33. Hulme, E. C., Birdsall, N. J., and Buckley, N. J. (2000) *Annu. Rev. Pharmacol. Toxicol.* **30**, 633–673
34. Caulfield, M. P., and Birdsall, N. J. (1998) *Pharmacol. Rev.* **50**, 279–290
35. Daaka, Y., Luttrell, L. M., and Lefkowitz, R. J. (1997) *Nature* **390**, 88–91
36. Felsch, J. S., Cachero, T. G., and Peralta, E. G. (1998) *Proc. Natl. Acad. Sci. U. S. A.* **95**, 5051–5056
37. Chan, D. A., Sutphin, P. D., Denko, N. C., and Giaccia, A. J. (2002) *J. Biol. Chem.* **277**, 40112–40117
38. Richard, D. E., Berra, E., Gothié, E., Roux, D., and Pouysségur, J. (1999) *J. Biol. Chem.* **274**, 32631–32637
39. Sang, N., Stiehl, D. P., Bohensky, J., Leshchinsky, I., Srinivas, V., and Caro, J. (2003) *J. Biol. Chem.* **278**, 14013–14019
40. Soucek, T., Cumming, R., Dargusch, R., Maher, P., and Schubert, D. (2003) *Neuron* **39**, 43–56
41. Hamilton, S. E., and Nathanson, N. M. (2001) *J. Biol. Chem.* **276**, 15850–15853
42. Oosthuyse, B., Moons, L., Storkebaum, E., Beck, H., Nuyens, D., Brusselmans, K., Van Dorpe, J., Hellings, P., Gorselink, M., Heymans, S., Theilmeier, G., Dewerchin, M., Laudenbach, V., Vermylen, P., Raat, H., Acker, T., Vleminckx, V., Van Den Bosch, L., Cashman, N., Fujisawa, H., Drost, M. R., Sciot, R., Bruyninckx, F., Hicklin, D. J., Ince, C., Gressens, P., Lupu, F., Plate, K. H., Robberecht, W., Herbert, J. M., Collen, D., and Carmeliet, P. (2001) *Nat. Genet.* **28**, 131–138

Targeting hypoxic cancer cells with a protein prodrug is effective in experimental malignant ascites

MASAHIRO INOUE[1], MUTSUKO MUKAI[1], YUKOU HAMANAKA[1], MASAHARU TATSUTA[2], MASAHIRO HIRAOKA[3] and SHINAE KIZAKA-KONDOH[4]

Departments of [1]Biochemistry, [2]Gastrointestinal Oncology, Osaka Medical Center for Cancer and Cardiovascular Diseases, Osaka 537-8511; Departments of [3]Therapeutic Radiology and Oncology, [4]Molecular Oncology, Kyoto University Graduate School of Medicine, Kyoto 606-8507, Japan

Received March 4, 2004; Accepted April 30, 2004

Abstract. Tumor hypoxia in a solid tumor mass has long been recognized as a cause of resistance to current cancer therapies, and has also been suggested to be a potent driving force towards malignancy. Recent progress in the understanding of the molecular mechanism of the tumor response to hypoxia has increased attention on targeting hypoxia for cancer therapy. We have generated a hypoxia-targeting fusion protein, TOP3, which is composed of a protein transduction domain (PTD) of HIV TAT, an oxygen-dependent degradation domain (ODD) of HIF-1α, and procaspase-3. Here, we examine the effects of TOP3 in a rat ascites model. First, we clarified that the fluid in ascites from MM1 cells, which are derivatives of AH130 rat ascites hepatoma cells, was highly hypoxic. *In vitro*, MM1 cells retained protein degradation machinery through the ODD domain, and TOP3 effectively impaired MM1 cell growth in culture under hypoxic conditions by inducing apoptosis. Intraperitoneal administration of TOP3 prolonged the life span of rats bearing a significant amount of malignant ascites, and 60% of the treated animals were cured without recurrence of ascites. Thus, TOP3 had a dramatic effect on malignant ascites and, hence, we propose that rodent malignant ascites is an appropriate platform for testing hypoxia-targeted drugs.

Correspondence to: Dr M. Inoue, Department of Biochemistry, Osaka Medical Center for Cancer and Cardiovascular Diseases, 1-3-3 Nakamichi, Higashinari-ku, Osaka 537-8511, Japan
E-mail: inoue-ma2@mc.pref.osaka.jp

Abbreviations: PTD, protein transduction domain; ODD, oxygen-dependent degradation domain; HIF, hypoxia inducible factor; VEGF, vascular endothelial growth factor; GFP, green fluorescent protein; NLS, nuclear localizing signal; HO, heme oxygenase; GLUT1, glucose transporter-1; PCR, polymerase chain reaction; mRNA, messenger RNA

Key words: hypoxia, ascites, apoptosis, caspase-3, HIF-1α

Introduction

Tumor hypoxia is of critical importance in tumor physiology and cancer treatment, and it appears to be strongly associated with malignant progression and resistance to therapy. Low oxygen levels in tumors are associated with increased metastasis, prompting gene mutations, such as those in p53 (1,2), and stimulating increased expression of genes favoring tumor survival and motility (3,4). Hypoxia has long been known to reduce the cytotoxic effects of ionizing radiation and, in some cases, of anticancer drugs (5). However, driven by the recent dramatic progress in the molecular understanding of the tumor hypoxia response, various strategies for molecular targeting of hypoxic cancer cells are emerging (6), such as blocking of the HIF-1α (hypoxia inducible factor 1α) signal (7).

Since HIF-1α has been shown to be a key molecule in hypoxic response for both normal and malignant cells, the HIF-1α signal is potentially a suitable target for hypoxia-targeted therapy. However, HIF-1α is a multifunctional transcription factor, and the results of targeting the signal in tumor cells are therefore rather unpredictable. Indeed, a recent report demonstrated that the signal can work as either a positive or negative regulator of tumor growth, depending on the cell type and the microenvironment (8).

Utilization of the death signal, which is elevated in cancer cells under hypoxic conditions, through caspase activation provides an alternative approach for targeting hypoxic cancer cells. We have generated a novel hypoxia-targeting protein, TOP3 (TAT-ODD-procaspase-3) (9). TOP3 consists of three components: PTD; the protein transduction domain of HIV TAT protein that enables the fusion protein to be non-specifically transferred into the cell, ODD; the oxygen-dependent degradation domain of HIF-1α that regulates the stability of the fusion protein, depending on the intra-cellular oxygen concentration, and procaspase-3, which is an inactive precursor of the executioner protease in apoptosis. Although tumor cells are resistant to the hypoxia-induced cell death signal, TOP3 induces the death of hypoxic tumor cells through caspase activity, which is induced by hypoxic stress, following transformation of the supplemented procaspase-3 into active caspase-3. Thus, TOP3 induces cell death only in hypoxic

malignant cells, and not in oxygenated normal cells. We have previously reported that i.p. administration of TOP3 moderately inhibited solid tumor growth without any significant side effects (9).

Ascites tumor cells have long been known to adapt and grow under severe hypoxia (10), providing a large number of homogeneous hypoxic cells. The cells in ascites fluid are potently anti-apoptotic under extreme hypoxia, under acidosis and at low glucose levels, recapitulating, at least partly, the malignant features of cancer cells (1,2). In solid tumors, hypoxia is accompanied by a wide variety of compounding conditions, such as low pH and low concentration of nutrients (11). Since it is extremely hard to reproduce such complex conditions *in vitro*, malignant ascites provides a unique platform to evaluate a hypoxia-targeting drug *in vivo*.

In this study, we show that TOP3 inhibits the accumulation of malignant ascites in a rat model, and that TOP3 has a dramatic effect on hypoxic cancer cells *in vivo*.

Materials and methods

Cell and cell culture. MM1 is a derivative clone originating from AH130 rat ascites hepatoma cells (12). MM1 cells were cultured in M-MEM supplemented with 10% FCS. Hypoxia was achieved by incubating cells with 1% O_2 and 5% CO_2 in a Multigas Incubator (Astec, Fukuoka, Japan). Anoxic conditions were achieved using an AneroPack system (Mitsubishi Gas Chemical, Tokyo, Japan). The cells were cultured under the hypoxic or anoxic conditions for the time periods described in the text.

Animal model. To produce malignant ascites, we injected $2x10^7$ MM1 cells in 1 ml of phosphate-buffered saline (PBS) into the peritoneum of 6-week-old male Donryu rats (SLC, Hamamatsu, Japan). Cell viability was assessed by trypan blue staining. Ascites volume was measured as the sum of fluid volume gathered by suction and the weight gain of gauze with which the entire abdominal cavity was wiped. A cytologist who was not informed of any experimental details counted cells on smears of ascites fluid. TOP3 (3 mg/kg) or buffer alone was injected intraperitoneally on day 7, 9 and 12 after inoculation of the cancer cells. All animal studies were approved by the Animal Care and Use Committee of Osaka Medical Center for Cancer and Cardiovascular Diseases.

Body measurement method. Under anesthesia with slight diethyl ether inhalation, a rat was held by its tail, and then a photograph was taken front on with a digital camera (CoolPics; Nikon, Tokyo, Japan). The images were transferred to a personal computer and analyzed using Photoshop software (Adobe, San Jose, CA). The distance between the top of the penis and the cross point of the front limbs on the chest was designated as Y and the maximum width of the belly orthogonal to line Y was designated as X. The ratio of X:Y was calculated and is referred to as the abdominal ratio.

Plasmids and transfection. Retrovirus vector, pMXiresEGFP (13) and pMX-FL (14) were generous gifts from Dr Kitamura (University of Tokyo, Japan). pMX-NLS-ODD-EGFP was constructed by inserting a BstXI-digested PCR fragment containing NLS-ODD into the BstXI sites of pMX-FL. PCR was performed using the plasmid pGEX/3-0/Casp3WT (9) as a template and the oligonucleotides 5'-AACCCAGTGTGG TGGCACCATGGACCCTAAGAAGAAGAGGAAGAAGA ACCCATTTTCTACTCA-3' and 5'-GGTGCCACTGTGC TGGCTGCTGGAATACTGTAACTG-3' as primers. The initiation codon of the EGFP gene was mutated into ATA with a Quick Change mutagenesis kit (Stratagene, La Jolla, CA). The complete sequence was confirmed using an ABI PRISM 3100 Genetic Analyzer (Applied Biosystems, Foster City, CA). High titer retroviruses were produced using the packaging cell line Plat-E (15). For infection of MM1 cells, $4x10^5$ cells were mixed with 850 µl of virus stock containing Polybrene (8 µl/ml) and cultured in 12-well plates. After 16-h incubation, the cells were transferred into 20 ml of culture medium. Thereafter, cloning of the transfected cells was performed by the limiting dilution method.

Oxygen tension, pH, and glucose concentration of ascites. Ascites samples were drawn from the abdominal cavity by puncturing with heparin-containing syringes, and then immediately subjected to analysis (ABL 700 series, Radiometer, Copenhagen, Denmark) for oxygen tension, pH and glucose concentration. Since the oxygen tension was below sensitivity, we approximated it using the following method. Ascites fluid was analyzed using an oxygen measuring system with a Clark type electrode (System 203, Instech, Plymouth Meeting, PA). To obtain reference measurements, non-treated ascites plasma was drawn from the ascites fluid, and bubbled in an airtight glass bottle for 1 h with the reference gas: air, 1% O_2 (1% oxygen, 99% nitrogen) or 0% O_2 (pure nitrogen). The ascites plasma was drawn from each bottle without allowing contact with air, and analyzed immediately. The probe-off mode was adjusted to a value of zero, and the air bubbled plasma was assigned a value of 150. A value for a sample was recorded 15 min after it was injected into the monitoring cell when the value did not change for at least 1 min.

Real-time quantitative RT-PCR of hypoxia-inducible gene expression. The ascites fluid was first mixed with an excessive amount of erythrocyte lysis buffer (150 mM NH_4Cl, 15 mM $NaHCO_3$, and 0.1 mM EDTA2Na, pH 7.3) to remove erythrocytes. Total RNA from MM1 cells cultured under normoxic and hypoxic conditions and from ascites cells was extracted with TRIzol (Invitrogen, Carlsbad, CA). The RNA was reverse transcribed to obtain cDNA using Ready-To-Go beads (Amersham Bioscience, Tokyo, Japan). Probe primer sequences for all rat genes are as follows: VEGF-A 5'-TGTACCTCCA CCATGCCAAGT-3', 5'-TGGAAGATGTCCACCAGGGT-3'; GLUT-1 5'-CTTTGTGTCTGCCGTGCTTA-3', 5'-CACATA CATGGGCACAAAGC-3'; HO-1 5'-CACGCATATACCCG CTACCT-3', 5'-AAGGCGGTCTTAGCCTCTTC-3'. Real-time quantitative PCR reactions were run in 96-well plates in an iCycler iQ Real-Time PCR Detection System (Bio-Rad, Hercules, CA), using iQ SYBR Green supermix (Bio-Rad) according to the manufacturer's protocol. RT-PCR conditions were 3 min at 95°C, 40 cycles of 15 sec at 95°C and 1 min at 62°C, followed by a step of 60°C for 1 min. Each sample was run in triplicate. The level of expression was standardized to

the primer set specific for rat ß-actin (5'-CCTGAGGAGC ACCCTGTG-3', 5'-AACACAGCCTGGATGGCTAC-3'). The $2^{-\Delta\Delta c_T}$ method was applied for the analysis of relative gene expression (16).

HIF-1α immunoblotting. Cultured MM1 cells and ascites cells were collected by centrifugation and the pellet was lysed with lysis buffer containing 10 mM Tris HCl (pH 7.2), 1 mM EGTA, 150 mM NaCl, 1% Triton X-100, 0.1% SDS, 1% sodium deoxycholate, 1 mM PMSF, and 50 mM sodium fluoride. Western blot analysis was performed as previously described (17). Briefly, proteins separated in an SDS-polyacrylamide gel (PAGE) were transferred electrophoretically to a PVDF membrane. The membrane was blocked with 5% non-fat dry milk solution in TBST, and incubated with a primary antibody against HIF-1α (HIα67; Novus, Littleton, CO) in TBST overnight at 4°C. After washing with TBST, the membrane was allowed to react with a secondary antibody (goat anti-mouse IgG; Santa Cruz Biotechnology, Santa Cruz, CA) conjugated with HRP (horseradish peroxidase). After extensive washing, signals were detected using ECL (Amersham Biosciences).

Preparation of the fusion proteins. The fusion proteins; TOP3 was prepared as previously described (9). Briefly, the plasmids (pGEX/3-0/Casp3WT) was transformed into BL21(DE3)pLysS (Novagen, Madison, WI), and the proteins were purified using Glutathione Sepharose 4B and PreScission Protease (Amersham Biosciences) following the manufacturer's instruction manual.

Flow cytometry. For EGFP degradation analysis, the cells were immediately fixed with 5% neutral buffered-formalin and rinsed twice with PBS. Cells in ascites fluid were centrifuged and treated with lysis buffer to remove erythrocytes and rinsed twice with PBS. The cells were analyzed on a Becton Dickinson FACSCalibur flow cytometer. Data were analyzed using CellQuest software (Becton Dickinson, San Jose, CA). Dead cells and debris were excluded based on forward-angle and side scatter. Ten thousand events were collected for each sample. Immunostaining was first performed with mouse anti-rat CD11b (MCA275R, Serotec, Oxford, UK) and then with a secondary antibody; Alexa Fluor 594, goat anti-mouse IgG (Molecular Probes, Eugene, OR).

Apoptosis and cell death assay. Caspase-3 activity was assayed with a CPP32 colorimetric Protease Assay Kit (BioVision, Mountain View, CA). To analyze the DNA content, MM1 cells ($1x10^6$ cells/5 ml in a 6-well plate) were pre-incubated for 18 h under normoxic (21% O_2) or hypoxic (1% O_2) conditions, and then various amounts of TOP3 protein were added to the medium. The cells were further cultured for 24 h under the same conditions as for the pre-incubation. Then the cells were harvested with centrifugation and the cell pellet was gently suspended in PBS and mixed with an equal volume of 2X hypotonic fluorochrome solution (100 mg/ml PI in 0.2% sodium citrate - 0.2% Triton X-100) immediately before analysis by flow cytometry using CellQuest (Becton Dickinson). For the DNA ladder, the same cell suspension used to analyze DNA content was treated with a DNA ladder detection kit (Roche Diagnostics, Mannheim, Germany) according to the manufacturer's instructions.

Statistical analysis. Statistical analysis was performed with GraphPad Prism 4 (GraphPad Software, San Diego, CA). The statistical significance of the results was tested with an unpaired-t, one-way ANOVA, a linear regression test, or a log-rank test for survival, depending on the hypothesis. $p<0.05$ was considered to be statistically significant.

Results

MM1 cell-induced malignant ascites fluid is hypoxic. Experimental malignant ascites cells are known to grow under severe hypoxia, under acidosis and at low glucose concentrations. Del Monte reported that ascites fluid produced by AH130, the parent cell line of MM1, was nearly anaerobic (18). To characterize the MM1 cell ascites, we performed the following analysis. First, we measured the oxygen tension of the ascites fluid on day 9. As shown in Fig. 1A, the oxygen level in the ascites fluid was >1%, compared with the oxygen level of ascites plasma saturated with gas containing 1% oxygen.

Next, to confirm the hypoxic response of the MM1 cells in ascites fluid, we examined expression levels of the known hypoxia-inducible genes, VEGF-A (vascular endothelial growth factor A) (19), GLUT-1 (glucose transporter-1) (20) and HO-1 (hemeoxygenase-1) (21) by real-time quantitative RT-PCR (Fig. 1B). The expression levels of both genes in cells recovered from ascites were higher than those in cells cultured under normoxic conditions, consistent with the pattern seen in cells cultured under hypoxic conditions. The expression of hypoxia inducible factor 1α (HIF-1α) is known to be regulated at the protein level (22). As shown in Fig. 1C, HIF-1α protein expression was upregulated in the ascites, although the mRNA level was slightly decreased (data not shown). The pH and glucose concentration of the ascites fluid on day 8 after injection were also examined. The pH value was 6.84±0.04 (n=5) and the glucose level was less than 2 mg/dl (n=5) (under the detection sensitivity).

Taken together, these results show that the ascites fluid produced by MM1 cells is hypoxic and has compounding conditions that include low pH and low glucose concentration. The results also show that the ascites cells are responsive to the hypoxic conditions.

Kinetics of the malignant ascites model. To investigate the kinetics of the animal model, we sacrificed the ascites-bearing animals at various time points, and measured the ascites fluid volume and the cell concentration. The total number of tumor cells in the ascites fluid was calculated by multiplying the ascites volume by the cell concentration. Both ascites volume and total cell number increased linearly from day 8 to day 13 (Fig. 2A and B). Thus, MM1 cells survive and proliferate in severely hypoxic conditions.

To evaluate the ascites volume without any further intervention, we established a body measurement method. Immediately after taking photographs for image analysis and determination of the abdominal ratio, we sacrificed the animals and measured the precise volume of the ascites fluid (see

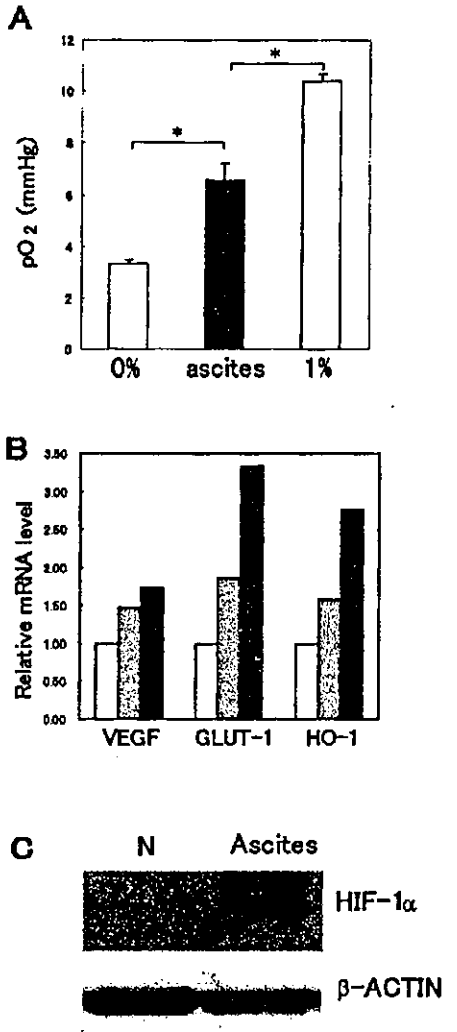

Figure 1. Malignant ascites produced by MM1 cells are hypoxic. (A), Low oxygen tension of ascites fluid from MM1 cells. Oxygen tension was measured in ascites fluid (ascites) on day 9 after inoculation and in ascites plasma bubbled with pure nitrogen (0% O_2) or a 1% oxygen and 99% nitrogen mixture (1% O_2). Values are mean ± SD; *p<0.01 compared with the ascites oxygen level by Student's t-test, n=3. (B), Elevated messenger RNA level of known hypoxia response genes in the ascites cells. The mRNA levels of VEGF-A, GLUT-1 and HO-1, which are known hypoxia response genes, were examined in cells cultured under 1% O_2 (gray bar) and in ascites cells (black bar) by real-time RT-PCR, normalized to the level of ß-actin, and represented as the fold increase over the levels of each gene under normoxic conditions (open bar). (C), Elevated level of HIF-1α protein in the ascites cells. Western blotting of the cell extract from MM1 cells cultured under normoxia (N) or from ascites cells (ascites) was performed with anti-HIF-1α antibody. The membrane was stripped and re-probed with anti-ß-actin antibody.

Materials and methods). Linear regression analysis showed that fluid volume and body size was significantly correlated with a p-value of <0.001. Hence, the body size is reliable for approximating the ascites volume (Fig. 2C).

Protein instability via ODD is functional in MM1 cells in vitro. To assess whether the protein degradation system through ODD is maintained in MM1 cells, a plasmid vector, pMX/NLS-ODD-EGFP was stably transfected into MM1 cells as a reporter. Green fluorescent protein (GFP) is suitable for comparing protein stability under hypoxia and normoxia as GFP chromophore formation is only impaired at near-anoxic conditions (23). The reporter plasmid contained the same HIF-1α ODD domain as TOP3, so that the fusion protein, NLS-ODD-EGFP, should be unstable at a normal oxygen concentration if protein degradation by the pVHL-proteasome system occurs in MM1 cells. Hence, the fluorescence signal should be weaker under normoxia than under hypoxia. As shown in Fig. 3, control vector-transfected cells had the same or slightly reduced fluorescence under hypoxia as under normoxia, while in two clones that were examined, the green fluorescence intensity was stronger under hypoxia than normoxia. Similar results were obtained when the cells were cultured with cobalt chloride (Sigma-Aldrich, Tokyo, Japan) as a hypoxic mimic. These results imply that the ODD domain in TOP3 is functionally preserved in MM1 cells.

TOP3 induces cell death in vitro. Caspase-3 is an executioner protease that is first produced as an inactive form, procaspase-3. With an apoptotic signal, procaspase-3 is cleaved into its active form by upstream initiator caspases, and then the active protease cleaves vital molecules to complete the programmed cell death (24). Hence, upon delivery into the target hypoxic cancer cells, the procaspase-3 of TOP3 should be activated to destroy the cells. To examine the upstream signals that activate procaspase-3, we first examined the endogenous caspase-3 activity in hypoxic cells (Fig. 4A). The hypoxic MM1 cells showed about 3-fold higher activity than the normoxic cells. Since MM1 cells underwent low but detectable apoptosis under hypoxic conditions (Fig. 4B), it is possible that the hypoxic stress stimulated the caspase cascade signal to the degree of activating procaspase-3 in hypoxic MM1 cells. Indeed, on adding TOP3 to MM1 cell culture medium, the caspase-3 activity elevated dose-dependently under hypoxic conditions. In contrast, no significant elevation of caspase-3 activity was observed under normoxia. Taken together, the above results suggest that TOP3 is stabilized only under hypoxic conditions and is activated by hypoxic stress, through which endogenous procaspase-3 is also activated to some degree.

We next examined TOP3-induced apoptosis. MM1 cells were cultured in hypoxic or normoxic conditions and then treated with various concentrations of TOP3. First, the subG1 population was assessed by flow cytometry. As shown in Fig. 4B, the subG1 population increased dose-dependently under hypoxia, while no change was observed under normoxia, even with a high dose of TOP3. Next, the same samples were examined for DNA ladders. With TOP3, DNA fragmentation by apoptosis increased dose-dependently under hypoxia (Fig. 4C). These results show that TOP3 enhances apoptosis of MM1 cells under hypoxic conditions *in vitro*.

TOP3 is effective in an in vivo ascites model. We were encouraged by the results *in vitro*, and we went on to test TOP3 *in vivo*. No toxic effect was observed in healthy animals. In the experiment shown in Fig. 5A, all (nine out of nine) ascites-bearing animals treated with the buffer died within 17 days after tumor cell inoculation. In contrast, treated animals lived longer and had a decreased ascites volume. Six out of